ARCAS ROCKET INSTRUMENTATION DEVELOPMENT FOR MESOSPHERIC MEASUREMENTS

Kay D. Baker, et al

Utah State University

Prepared for:

Air Force Cambridge Research Laboratory

June 1972

AFCRL 72-0472

space science laboratory

Arcas Rocket Instrumentation Development for Mesospheric Measurements

by

Kay D. Baker and Glenn D. Allred

SCIENTIFIC REPORT NO. 1

JUNE 1972

Contract No. F19628-70-C-0302
Project No. 7663
Task No. 766303
Work Unit No. 76630301

Prepared for Air Force Cambridge Research Laboratories
Air Force Systems Command, United States Air Force
Bedford, Massachusetts 01730

Contract Monitor: James C. Ulwick
Ionospheric Physics Laboratory

Approved for public release; distribution unlimited.

UTAH STATE UNIVERSITY

CENTER FOR RESEARCH IN AERONOMY LOGAN, UTAH 84322

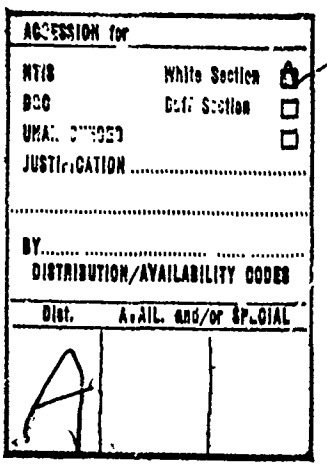

Qualified requestors may obtain additional copies from the Defense Documentation Center. All others should apply to the National Technical Information Service.

Unclassified
Security Classification

DOCUMENT CONTROL DATA - R & D

(Security classification of title, body of abstract and indexing annotation must be entered when the overall report is classified)

1. ORIGINATING ACTIVITY (Corporate author)	2a. REPORT SECURITY CLASSIFICATION
Space Science Laboratory Utah State University Logan, Utah 84322	Unclassified
	2b. GROUP

3. REPORT TITLE

ARCAS ROCKET INSTRUMENTATION DEVELOPMENT
FOR MESOSPHERIC MEASUREMENTS

4. DESCRIPTIVE NOTES (Type of report and inclusive dates)

Scientific Interim

5. AUTHOR(S) (First name, middle initial, last name)

Kay D. Baker
Glenn D. Allred

6. REPORT DATE	7a. TOTAL NO. OF PAGES	7b. NO. OF REFS
June 1972	~~68~~ 70	13

8a. CONTRACT OR GRANT NO.	9a. ORIGINATOR'S REPORT NUMBER(S)
F19628-70-C-0302	
b. Project, Task, Work Unit Nos. 7663-03-01	Scientific Report No. 1
c. DoD Element 62101F	9b. OTHER REPORT NO(S) (Any other numbers that may be assigned this report)
d. DoD Subelement 687663	AFCRL-72-0472

10. DISTRIBUTION STATEMENT

A - Approved for public release; distribution unlimited.

11. SUPPLEMENTARY NOTES	12. SPONSORING MILITARY ACTIVITY
TECH, OTHER	Air Force Cambridge Research Laboratories (LI) L. G. Hanscom Field Bedford, Massachusetts 01730

13. ABSTRACT

This program for development of small rocket probes and mesospheric research was jointly sponsored by the Air Force Cambridge Research Laboratories and the Atmospheric Sciences Laboratory (Army Electronic Systems Division). The program entailed the development and use of payloads for studying prescribed mesospheric parameters using small, meteorological-type rockets as the probing vehicles, and was completed in two phases with launches at White Sands Missile Range, New Mexico, during June and July, 1971.

Three of the payloads were designed and fabricated for Air Force Cambridge Research Laboratories at the Space Science Laboratory, Utah State University, Logan, Utah. These three payloads utilized new techniques to measure atomic oxygen, Lyman-alpha radiation, 1.27-μ radiation from $\Theta_2(^1\Delta_g)$, and nitric oxide within the mesospheric region. The program served as an extremely significant step in the development and evaluation of the new instruments and techniques.

Each instrument's measurements philosophy, design and result is presented.

DD FORM 1 NOV 65 1473

Unclassified
Security Classification

14. KEY WORDS	LINK A		LINK B		LINK C	
	ROLE	WT	ROLE	WT	ROLE	WT
Small rocket instrumentation						
Mesospheric probes development						
Atmospheric probes						
Nitric oxide measurement techniques						
Atomic oxygen measurement techniques						
Lyman-alpha measurement techniques						
Cooled radiometer						

AFCRL-72-0472

ARCAS ROCKET INSTRUMENTATION DEVELOPMENT FOR MESOSPHERIC MEASUREMENTS

by

Kay D. Baker and Glenn D. Allred

Space Science Laboratory
Center for Research in Aeronomy
Utah State University
Logan, Utah 84322

Contract No. F19628-70-C-0302
Project No. 7663
Task No. 766303
Work Unit No. 76630301

SCIENTIFIC REPORT NO. 1

June 1972

Contract Monitor: James C. Ulwick
Ionospheric Physics Laboratory

Approved for public release; distribution unlimited

prepared for

Air Force Cambridge Research Laboratories
Air Force Systems Command
United States Air Force
Bedford, Massachusetts 01730

LIST OF CONTRIBUTORS -- SCIENTISTS AND ENGINEERS

K. D. Baker -- Principal Investigator

D. J. Baker

R. D. Briscoe

D. A. Burt

G. D. Frodsham

J. F. Kemp

G. K. LeBaron

L. R. Megill

E. F. Pound

T. Tohmatsu

B. J. Wheeler

C. L. Wyatt

RELATED CONTRACTS AND PUBLICATIONS

F19628-67-C-0275

F19628-69-C-0007

Burt, D. A. and G. D. Allred, Rocket instrumentation for auroral measurements--Aerobee 3.756 and 3.759, *UARL Final Report, AFCRL 70-0658*, 193 pp., Contract F19628-69-C-0007, Upper Air Research Laboratory, University of Utah, Salt Lake City, November 1970.

Baker, K. D., D. A. Burt, L. C. Howlett and G. D. Allred, Rocket instrumentation for the study of a polar cap absorption event -- PCA-69, *UARL Final Report, AFCRL 70-0251*, 270 pp., Contract F19628-67-C-0275, Upper Air Research Laboratory, University of Utah, Salt Lake City, April 1970.

PREFACE

At Utah State University a number of individuals had specific responsibilities for various phases of this project.

Principal Investigator and Project Scientist	K. D. Baker
Payload Consulting Engineer	D. A. Burt
Scientific Advisor	L. R. Megill
Atomic Oxygen and Lyman-α Payload	B. J. Wheeler
1.27-μ Radiometer	J. F. Kemp
1.27-μ Radiometer Payload	L. K. Beckstead
Nitric Oxide and Ozone Measurements Scientific Advisor	T. Tohmatsu
Nitric Oxide Payload	L. D. Forsberg R. B. Smith
Airborne Telemetry	E. F. Pound D. R. Bunnell
Payload Fabrication	V. L. Carlson P. C. Neal M. E. Taylor
Field Operations	K. D. Baker B. J. Wheeler J. C. Kemp L. K. Beckstead L. D. Forsberg R. B. Smith G. K. LeBaron
Mobile Observatory	R. D. Briscoe
Assistant Administrator	J. O. Coleman
Documentation	G. D. Allred R. M. Fowler D. A. Brookshier

TABLE OF CONTENTS

TABLE OF CONTENTS (cont.)

LIST OF ILLUSTRATIONS

LIST OF ILLUSTRATIONS (cont.)

LIST OF TABLES

INTRODUCTION

Small sounding rockets of the Arcas and boosted-Arcas type are currently serving to revise some aspects of atmospheric research. These small, solid fuel rockets, developed originally for meteorological sounding of the lower atmosphere, provide a relatively inexpensive and convenient means of inserting measuring devices into the upper atmosphere for direct, *in situ* measurement of atmospheric parameters. Advances in the state of the art of miniaturization and packaging now make it possible to conduct significant aeronomic measurements with the small payloads. In use, simplified launching stations permit rapid launching of the vehicles by range personnel when appropriate events occur.

The small rockets, however, cannot attain extremely high altitudes and cannot be compared to the larger vehicles in payload complexity, but for experimentation within the mesospheric region (50-90 km) they can be equipped with experiments which well justify their use. Since the small rockets are widely used in meteorological applications, there is a widespread availability of launching sites which can accommodate the rockets even when they are used for purposes other than meteorology.

During the summer of 1971 these small rockets were used in a program designed primarily to investigate and improve mesospheric probing techniques that was jointly sponsored by Air Force Cambridge Research Laboratories (AFCRL) and Atmospheric Sciences Laboratory (ASL) of the Army Electronic Systems Division. As initially planned, the program consisted of ten instrumented small rockets, six sponsored by ASL and four by AFCRL. All of the planned experiments were related directly or through various processes, and the planned, near simultaneous launchings would provide an opportunity for the correlation and comparison of various measurements techniques. The program was initially scheduled to be conducted at the White Sands Missile Range, New Mexico, in June, 1971, with scheduling of vehicles and measurements as depicted in Table I.

TABLE I

MESOSPHERIC PROBE STUDIES ROCKET LAUNCH SCHEDULE

Vehicle	Scheduled Launch Time (Local)	Measurements	Technique	Experimenter
Sparrow-Arcas	0600	Nitric Oxide Concentration	Resonance Scattering Photometer (2150 Å)	AFCRL/USU
Super Arcas	0605	Atomic Oxygen Concentration Solar Lyman-α Radiation	Thin Film Silver Detector NO Ionization Chamber	AFCRL/USU
Sparrow-Arcas	0635	$O_2(^1\Delta_g)$ Concentration	Liquid Nitrogen Cooled IR Radiometer (1.27 μ)	AFCRL/USU
Arcas	0640	Ozone Concentration Temperature	Chemiluminescent Disc Thermistor (Parachute borne)	ASL
Sparrow-Arcas	0710	Ozone Concentration Electron Density	Absorption Photometer (2500 Å), Z-θ Probe, DC Probe	AFCRL/USU
Arcas	0715	Positive Ions	DC Blunt Probe (Parachute borne)	ASL/Penn State U.
Sidewinder-Arcas	0745	Electron Density	Faraday Rotation	ASL
Loki-Viper	0820	Air Density	Inflatable Sphere	ASL
Arcas	0905	Atmospheric Composition	Cryogenic Air Sample	ASL
Loki	1100	Temperature	Parachute Thermistor	ASL

In addition to the rocket measurements the USU mobile observatory was initially on site to perform supporting measurements of airglow.

Several rockets were launched according to this initial plan, but the inability to fire the Sparrow-Arcas igniters caused the postponement of the program until July, 1971. At that time the remainder of the measurements phase of the mesospheric probe program was completed.

As illustrated in Table I, four AFCRL payloads were designed for the mesospheric probes program. These payloads were designed and fabricated at Space Science Laboratory, Utah State University, Logan, Utah. One of the four payloads was launched in June when the first attempt at completing the program was made. Subsequently, one payload was removed from this program and was transferred to Thule, Greenland, to be utilized for poalr cap absorption event measurements. The two remaining AFCRL payloads flew in July, 1971, at White Sands when the program was completed.

In overview, through cooperation by experimenters, the mesospheric probes program afforded atmospheric scientists the opportunity to participate in a coordinated attack directed toward both developing small rocket measuring techniques and obtaining correlating measurements. Both new and proven instruments were utilized to perform the measurements. Such a program has inherent advantages in that many of the measurements are of related parameters. This not only provides the opportunity to obtain the measurements themselves, but additionally makes possible the opportunity to cross-evaluate the probes and measurements through correlation, thereby providing checks of technique validity and feasibility. The remainder of this report will be confined to a detailed discussion of the AFCRL/USU payloads flown at White Sands.

AREAS OF INVESTIGATION AND MEASUREMENTS PHILOSOPHY (AFCRL/USU Payloads)

Atomic Oxygen Concentration

Accurate measurements of atomic oxygen concentrations as a function of altitude above the earth's surface are essential to an understanding of the important controlling reactions entered into by this

extremely active atmospheric species. Atomic oxygen is recognized as one of the main energy storage systems for the solar radiation absorbed in the earth's upper atmosphere and plays a dominant role in determining the energy balance within this region. Atomic oxygen is primarily formed from the less reactive O_2 molecule, dominantly by dissociation due to photolysis (by solar ultraviolet radiation) by the reaction

$$O_2 + h\nu \longrightarrow O + O$$

O_2 exhibits its greatest cross-section for photolysis in the region of the Schumann-Runge continuum (1760 Å - 1926 Å) of the electromagnetic spectrum, and therefore, this solar ultraviolet radiation is the prime producer of O. Other secondary reactions also produce O, among them the reaction

$$O_3 + h\nu \longrightarrow O + O_2$$

is important in determining the overall O concentration. This reaction is also the result of photon absorption in the ultraviolet portion of the solar spectrum (2000 - 3000 Å).

As can be seen from the graph shown in Figure 1, atomic oxygen formed by UV radiation extends over a large range of altitudes with the greatest concentrations exhibited in the vicinity of 100 km. This is substantiated by the information in Figure 2, a model which shows a theoretical comparison of day and night O concentrations for various altitudes (adapted from *Hunt* [1966]). The large variation between day and night concentrations in the lower regions is due to the recombination reactions and is measurable on a diurnal basis. The concentrations remain relatively constant in the higher altitudes since the rate of loss of O is small at higher altitudes due to the requirements of the third body in the reactions.

$$O + O + M \longrightarrow O_2 + M$$

$$O + O_2 + M \longrightarrow O_3 + M$$

These recombination reactions, therefore, determine the lifetime of the O atoms. Downward diffusion of O created at the higher altitudes to levels where significant recombination takes place is the primary means

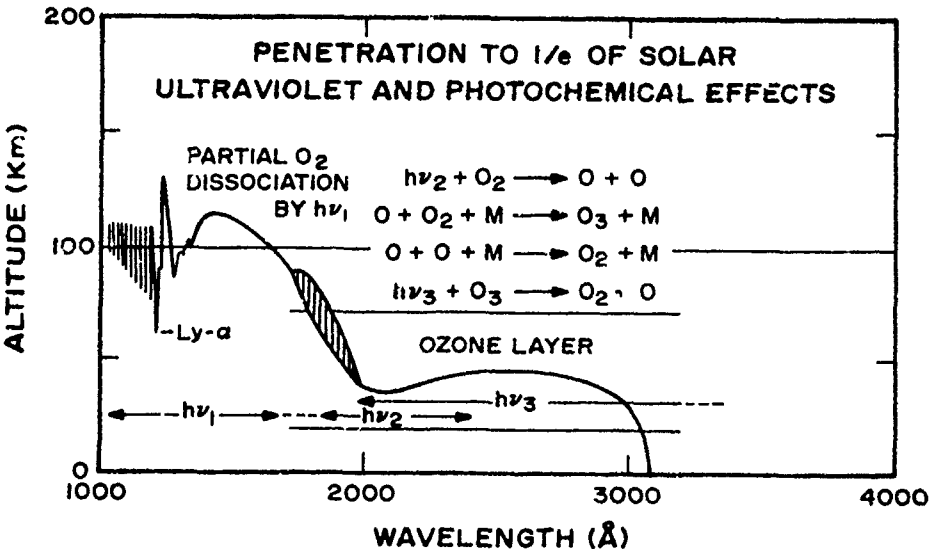

Figure 1. Atmospheric penetration to $\frac{1}{e}$ of solar ultraviolet radiation and the resulting photochemical effects within the atmosphere as related to height and wavelength.

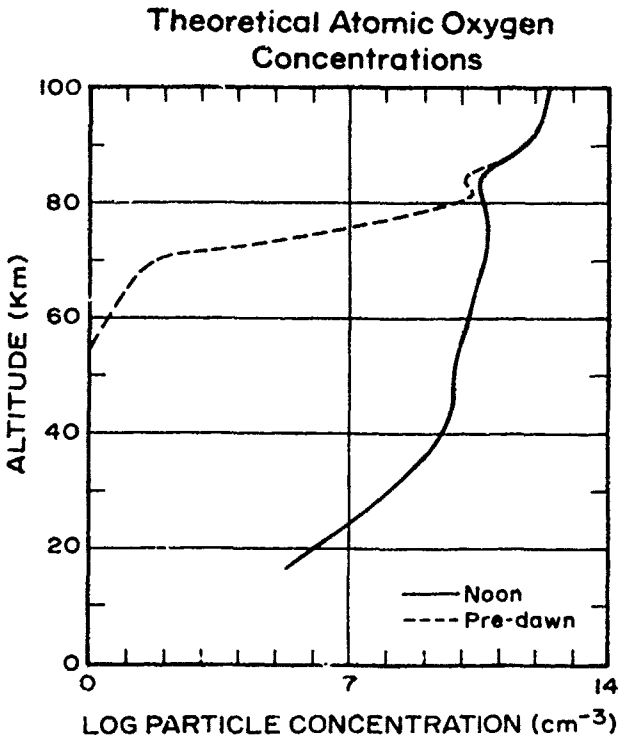

Figure 2. A theoretical model of atomic oxygen concentration vs. altitude for noon and pre-dawn conditions (adapted from *Hunt* [1966]).

by which the concentrations at high altitudes are modified and stabilized. Incidentally, Figure 1 also shows the altitude location of the O_3 layer which is formed by the reaction shown above and in turn through absorption and 0 production, prevents the dangerous UV radiation from reaching the earth's surface.

Accurate measurement of mesospheric 0 concentration is extremely difficult as a result of two characteristics. First, atomic oxygen is a very minor atmospheric constituent. Throughout the homosphere (altitudes to approximately 90 km) atmospheric composition remains relatively constant with Nitrogen (N_2) comprising approximately 78% of the atmosphere, Oxygen (O_2) 21%, and Argon ½%, The remaining ½% is made up of all other atmospheric constituents including a small fraction of 0. Above about 90 km these percentages do not remain constant, and in fact, 0 concentrations increase until at about 120 km the density of atomic oxygen becomes equal to that of molecular oxygen. In the lower altitude range especially, instrument sensitivity must be high to obtain measurements. Secondarily, the reactive nature of 0 compounds the difficulty of obtaining measurements since 0 is destroyed by surface reactions. Therefore, the very presence of a measuring instrument is a disruptive element and can be the cause of erroneous measurements. Due to these factors, measurements of atomic oxygen in the atmospheric region below 100 km are virtually nonexistant, and analysis of atmospheric conditions has been dependent upon theoretical models rather than accumulated data.

The atomic oxygen measurement technique utilized in the mesospheric probes program, however, is designed to take advantage of the highly reactive nature of the 0 species and measure the effect of the reaction rather than measure the 0 directly as described in the instrumentation section.

Lyman-Alpha Radiation (1216 Å)

The prominent solar Lyman-alpha emission from hydrogen at 1216 Å is extremely important in D-region atmospheric chemistry. It is the principle mechanism for mid-D-region ionization because it falls in an

O_2 absorption minimum allowing it to penetrate to that depth (see Figure 1), and the Lyman-alpha radiation contains sufficient energy to ionize the minor atmospheric constituent Nitric Oxide. With the removal of the Lyman-alpha ionizing source at nighttime, the ionospheric D-region disappears in quiet times. Accurate measurement of Lyman-alpha radiation intensity at various altitudes under quiet ionospheric conditions can provide a more thorough understanding of the role of this ionizer in total atmospheric chemistry, and accordingly. instruments were included in this program to measure Lyman-alpha intensity.

$O_2(^1\Delta_g)$ Concentration (1.27-μ Radiation)

A knowledge of the concentration of metastable oxygen molecules in the D-region is important to the understanding of the chemical processes operative there. The $O_2(^1\Delta_g)$ state is particularly interesting because its long lifetime (approximately an hour) makes its excitation energy of nearly 1 ev available in interactions of many types. *Hunten and McElroy* [1968] pointed out that this excited state can be ionized by ultraviolet radiation in the wavelength band 1027-1118 Å, parts of which can penetrate below 70 km, and therefore is an important source of daytime ions. Although the possible importance of this mechanism appears to be diminished by the work of *Huffman, et al.* [1971] which includes absorption by CO_2, it should still be considered for overall D-region processes. Daytime production of $O_2(^1\Delta_g)$ is accomplished primarily by photolysis of ozone

$$O_3 + h\nu \longrightarrow O_2(^1\Delta_g) + O\ (^1D)$$

due to solar radiation in the Hartley continuum (2000-3000 Å). Considering this process in reverse leads one to the conclusion that one method of determining ozone concentration might be through measurement of $O_2(^1\Delta_g)$ band brightness (1.27 μ). This, of course, would only be possible during the daytime. At night the brightness of the IR atmospheric O_2 band at 1.27 μ is considerably reduced from that of the dayglow having a value under quiet nighttime conditions of about 90 kR.

The production of $O_2(^1\Delta_g)$ at night has been assumed [*Gattinger*, 1971] to be due to the reaction

$$O(^3P) + O(^3P) + M \longrightarrow O_2(^1\Delta_g) + M$$

The dependence of the rate of this reaction upon the square of the $O(^3P)$ concentration predicts a maximum in the brightness of the $O_2(^1\Delta_g)$ band at an altitude of about 90 km. Additionally, anything that significantly affects the $O(^3P)$ concentration, such as atmospheric circulation or seasonal and/or diurnal dependence, also effects the brightness of 1.27-μ radiation due to this production process. Here again, conclusive evidence that the O + O + M process is the dominant $O_2(^1\Delta_g)$ production process could possibly lead to a means of determining O concentration by measuring the brightness of the 1.27-μ radiation. Several other mechanisms involving excited $O_2(^1\Delta_g)$ molecules could be important to D-region chemistry: for example, the possible short-circuiting of the chain of reactions resulting in the hydration of ions [*Ferguson and Fehsenfeld*, 1970]. Finally, the importance of $O_2(^1\Delta_g)$ in auroras has not been determined. Although *Noxon* [1970], *Megill, et al.* [1970], and others have reported enhancements of 1.27-μ emission under various auroral conditions, a definite correlation between auroral activity and the enhancement of this band has not been established. That is to say, 1.27-μ emission appears to be strongly enhanced during some auroras and not so during others. Measurement of 1.27-μ radiation during quiet, undisturbed atmospheric conditions can provide reference information which will hopefully assist in defining the operative chemical processes.

Nitric Oxide

Although Nitric Oxide (NO) is a minor atmospheric constituent, it plays a dominant role in the formation of the ionospheric D-region as previously discussed, and its importance in atmospheric chemistry makes further study of this atmospheric specie desirable. The presence of NO in the upper atmosphere was first successfully verified experimentally by *Barth* [1964]. This experiment, utilizing a rocketborne, scanning ultraviolet photometer, demonstrated that the most outstanding

emission features in the spectral range between 2000-3000 Å were the γ-bands of NO, with the band at 2155 Å especially prominant. This prominant band in the day airglow is due to the resonance-fluorescence scattering of solar ultraviolet radiation by NO. The directional solar flux at 2155 Å is absorbed by NO which is excited by the absorption, and as the excited NO relaxes back to the ground state, it reradiates at 2155 Å, essentially redirecting and diffusing the solar flux.

As a result of the application of the ultraviolet scanning spectrometer, a few rocketborne measurements have been successful in indicating altitude distribution of NO in the upper atmosphere [*Barth*, 1966; *Pearce*, 1969; *Meira*, 1971], but the scanning UV spectrometer technique requires a large vehicle to carry the instrumentation; the instrumentation and payload are complex; and corresponding experimental costs are high.

A new device, designed to provide essentially the same information relating to atmospheric NO concentrations as that provided by the spectrometer technique but utilizing a new concept, was employed in the mesospheric probes program. The payload is small and relatively simple and is made so by exploiting the resonance-fluorescence characteristics of NO to achieve the measurements.

The foregoing discussions have described briefly some of the particulars associated with those atmospheric parameters which the AFCRL/USU payloads were designed to measure. The remaining sections of this report detail the instrumentation of each of the three AFCRL rockets and payloads which were actually utilized.

INSTRUMENTATION
(AFCRL/USU Payloads)

General

Table II provides overall information pertaining to the vehicle configuration, launch date and time, and instrumentation and measurements of each of the mesospheric payloads.

TABLE II

AFCRL/USU MESOSPHERIC ARCAS PAYLOAD

LAUNCH AND INSTRUMENTATION DETAILS

Payload/ Vehicle	Launch Date/ Time (local)	Instrumentation	Measurement
Arcas 71-2 Super Arcas	6/9/71 0605:00	NO Ionization Chamber	Solar Lyman-alpha Radiation (1216 Å)
		Silver Film Atomic Oxygen Detector	Integrated Atomic Oxygen Density
		Magnetometer	Payload Attitude
		Baroswitch	Coarse Trajectory
Arcas 71-3 Sparrow-Arcas	7/28/71 0615:00.3	Cooled IR Radiometer	1.27-μ Radiation-$O_2(^1\Delta_g)$
		Magnetometer	Payload Attitude
		Baroswitch	Coarse Trajectory
Arcas 71-4 Sparrow-Arcas	7/28/71 0649:58.9	UV Resonance-Scattering Photometer (2150 Å)	Integrated Nitric Oxide Concentration
		Magnetometer	Payload Attitude
		Baroswitch	Coarse Trajectory

Vehicles

Table II shows that two vehicle types were utilized in this program, i.e., Super Arcas and Sparrow-Arcas vehicles.

Super Arcas

The Super Arcas sounding vehicle provides a simple, versatile means for probing the mesosphere. The rocket motor uses an end-burning solid propellant configuration and can be launched from standard Arcas launchers installed at meteorological launch sites throughout the free world. Assembly and launch operations can be completed by a two-man crew.

The Super Arcas is launched from a closed-breech launcher which uses entrapped rocket exhaust gases to accelerate the vehicle along the launching tube. A launching piston attached to the nozzle end of the rocket provides a gas seal during travel, and plastic spacers center and support

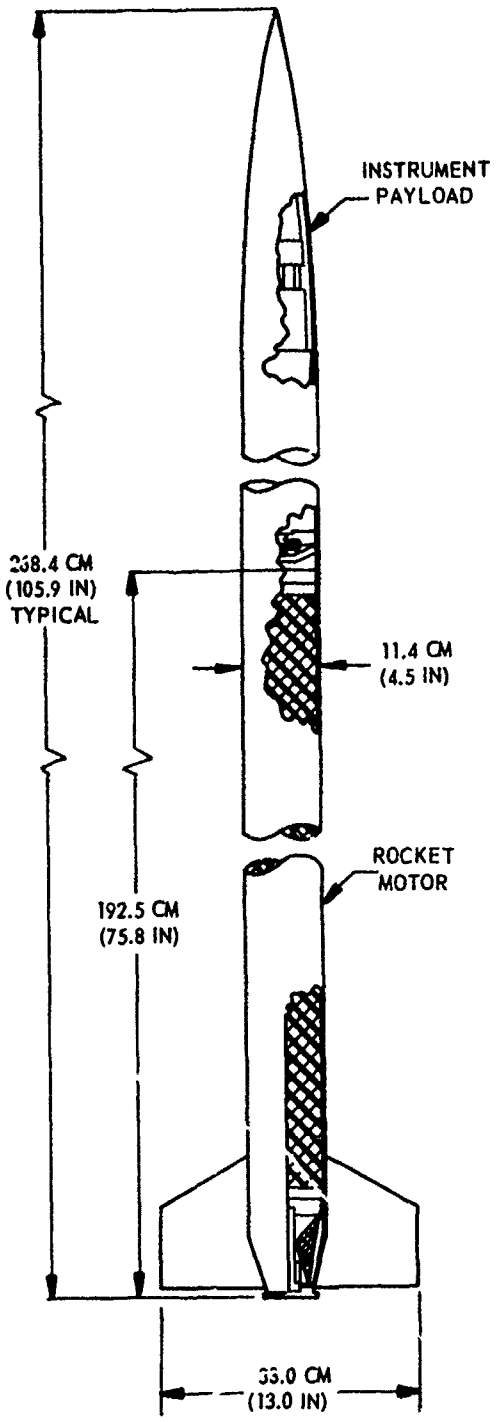

the rocket as it leaves the launching tube. With the standard 20-foot launching tube this system will impart a launching velocity of 150 feet-per-second to the vehicle with a peak acceleration load of 40 g and a nominal spin rate at burnout of 23 rps.

The launcher can be aimed through 360 degrees in azimuth and 180 degrees in elevation. Figure 4 shows two theoretical trajectories for rockets launched at sea level and compares the Super Arcas and Sparrow-Arcas capabilities. Figure 5 shows the apogee vs. ground range characteristics for three launch elevations and various payload weights.

A schematic drawing of a Super Arcas motor and payload configuration as used in the Arcas 71-2 application is shown in Figure 3.

Figure 3. A schematic diagram of the Super Arcas vehicle configuration.

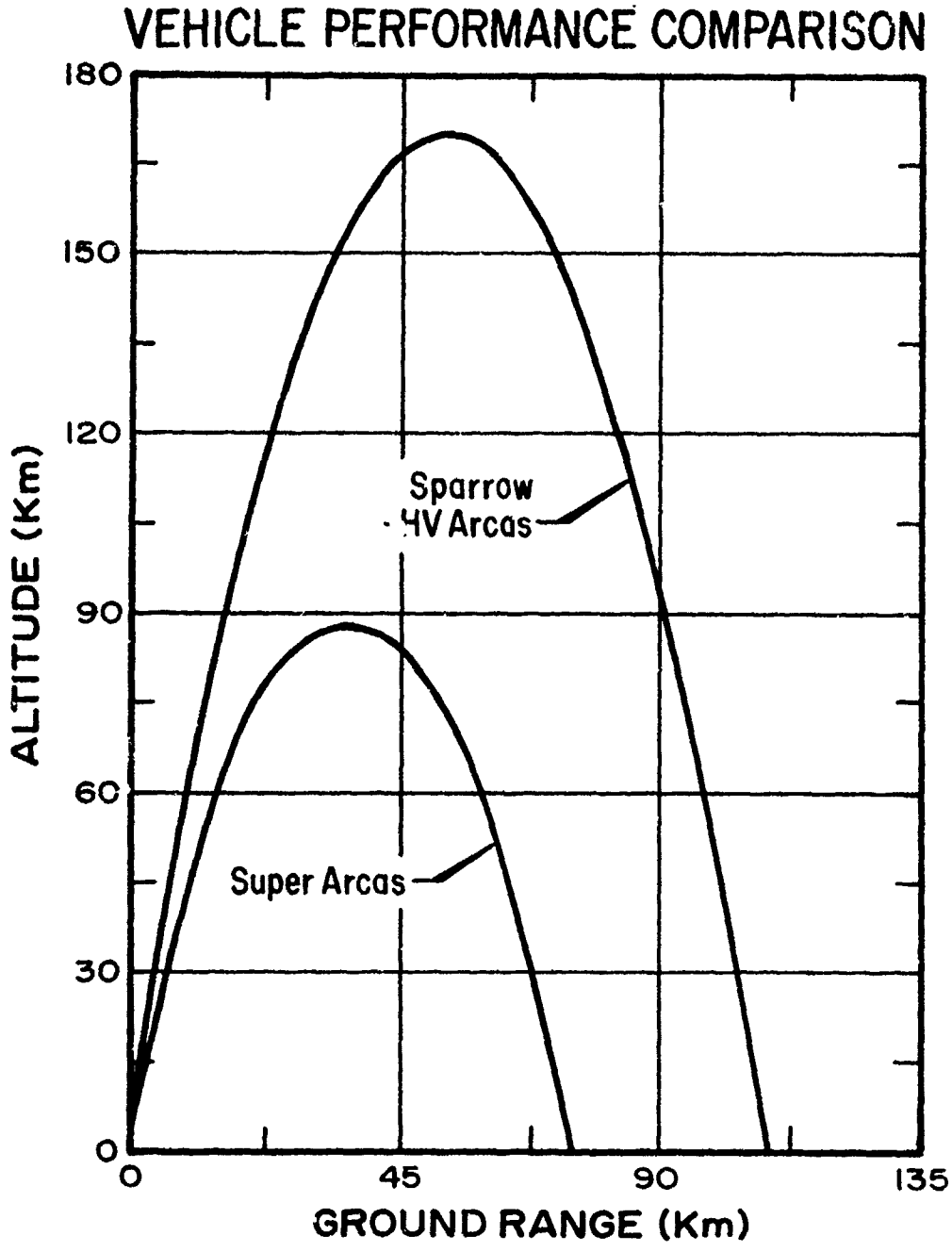

Figure 4. Super Arcas and Sparrow-Arcas vehicle performance comparisons (typical) for a sea-level launch at 84° elevation.

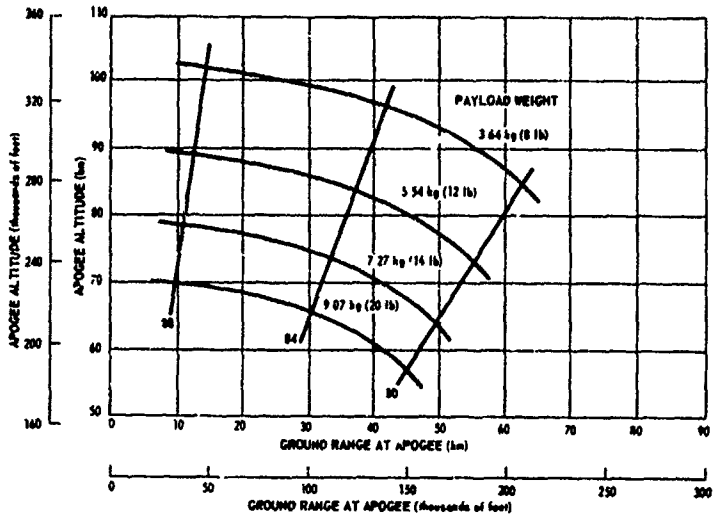

Figure 5. Super Arcas apogee vs. ground range characteristics for three typical launch elevations and various payload weights.

Sparrow Arcas

The second two rockets (Arcas 71-3 and 71-4) were of the Sparrow-Arcas configuration. This combination is shown in Figure 6. It utilizes an eight-inch diameter Sparrow Mark 6 Mod C-8 propulsion unit as a booster behind a MARC 2C1 HV (high velocity) Arcas.

Staging is accomplished by a bayonet-type interstage adapter that provides structural rigidity during boost, but permits drag-induced stage separation. Fin assemblies are preset to provide an approximate spin rate of 20 rps at second-stage burnout.

The Sparrow Arcas launch system is a 15-foot long rail assembly designed for mounting on an adjustable boom launcher of the type available at most launch sites. Assembly and launch preparation require no special handling equipment.

Power for ignition of both stages is provided by a ground source; a motion switch completes the second stage firing circuit only after

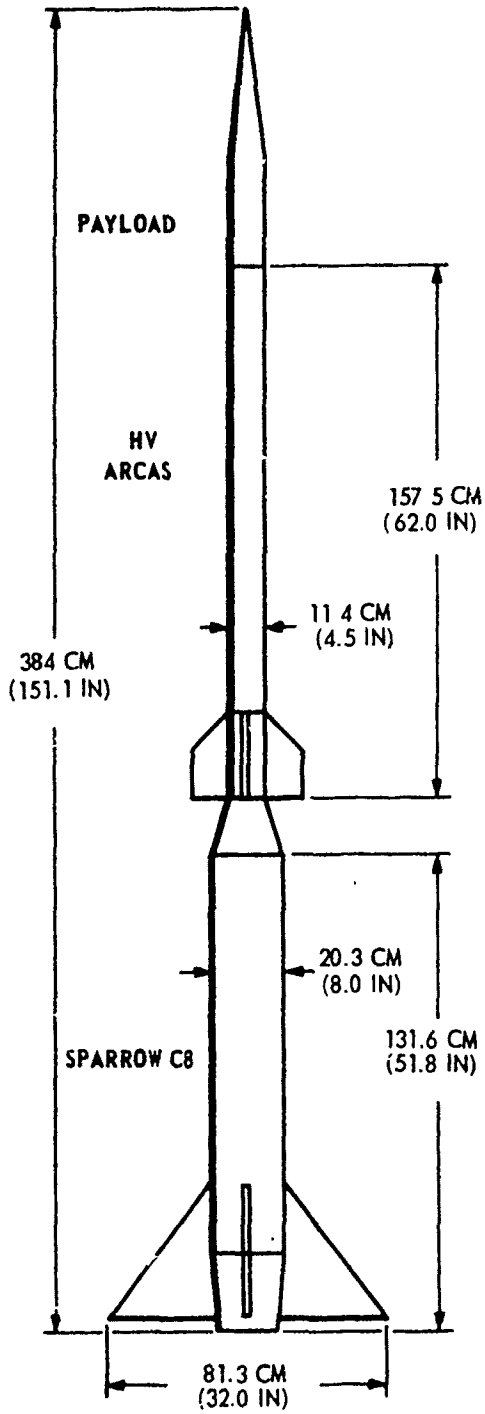

positive booster ignition. A delay squib in the second stage igniter allows six seconds of coasting flight between booster burnout and second stage ignition.

Figure 7 shows some typical apogee vs. ground range capabilities for various launch angles and payload weights and Figure 4 shows theoretical trajectories for Sparrow-Arcas vehicles.

Payloads

Because the three mesospheric probe payloads were not closely related in major design or physical aspects, separate discussions of the instrumentation included in each payload are required. The remainder of this report is divided into four sections. Three of these sections deal individually with each payload. These three sections are preceded by a section which deals with their one common factor, the separable nosetip assembly.

Figure 6. A schematic diagram of the Sparrow-Arcas vehicle configuration.

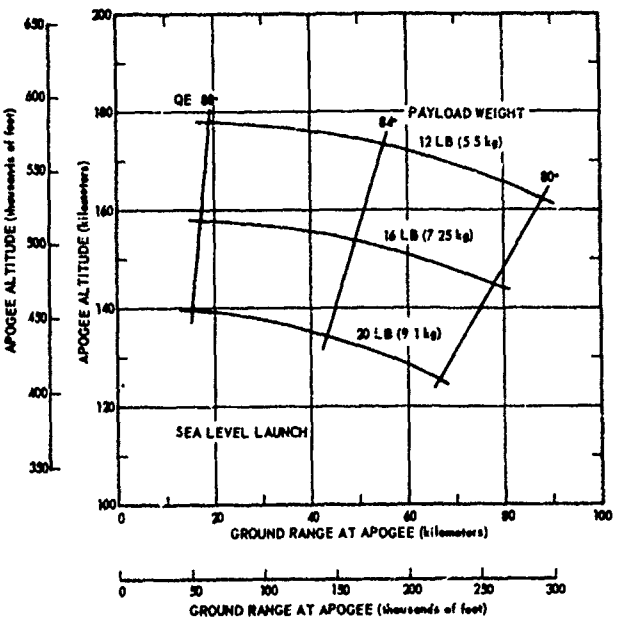

Figure 7. Sparrow-Arcas apogee vs. ground range characteristics for three typical launch elevations and various payload weights.

Separable Nosetip Assembly, ARCAS 71-2, 71-3, and 71-4

Each of the three mesospheric probes were equipped with instruments which looked in the direction of the vehicle major axis. This configuration requires a protective device (the vehicle nosetip) which can be ejected to expose the instrument when the vehicle has traversed the more dense portion (lower layers) of the atmosphere. This protection and ejection was similarly accomplished in all three of the mesospheric probe payloads. Figure 8 describes the method of nosetip separation utilized for these payloads. As can be seen from the figure, the separable nosetip is a clamshell device which is separated into two portions at the time of ejection. The device incorporates timers that fire a guillotine type bolt cutter at a predetermined time to achieve the separation. The horizontal velocity required to accomplish the separation is imparted by the guillotine and by centrifugal force generated by rocket spin.

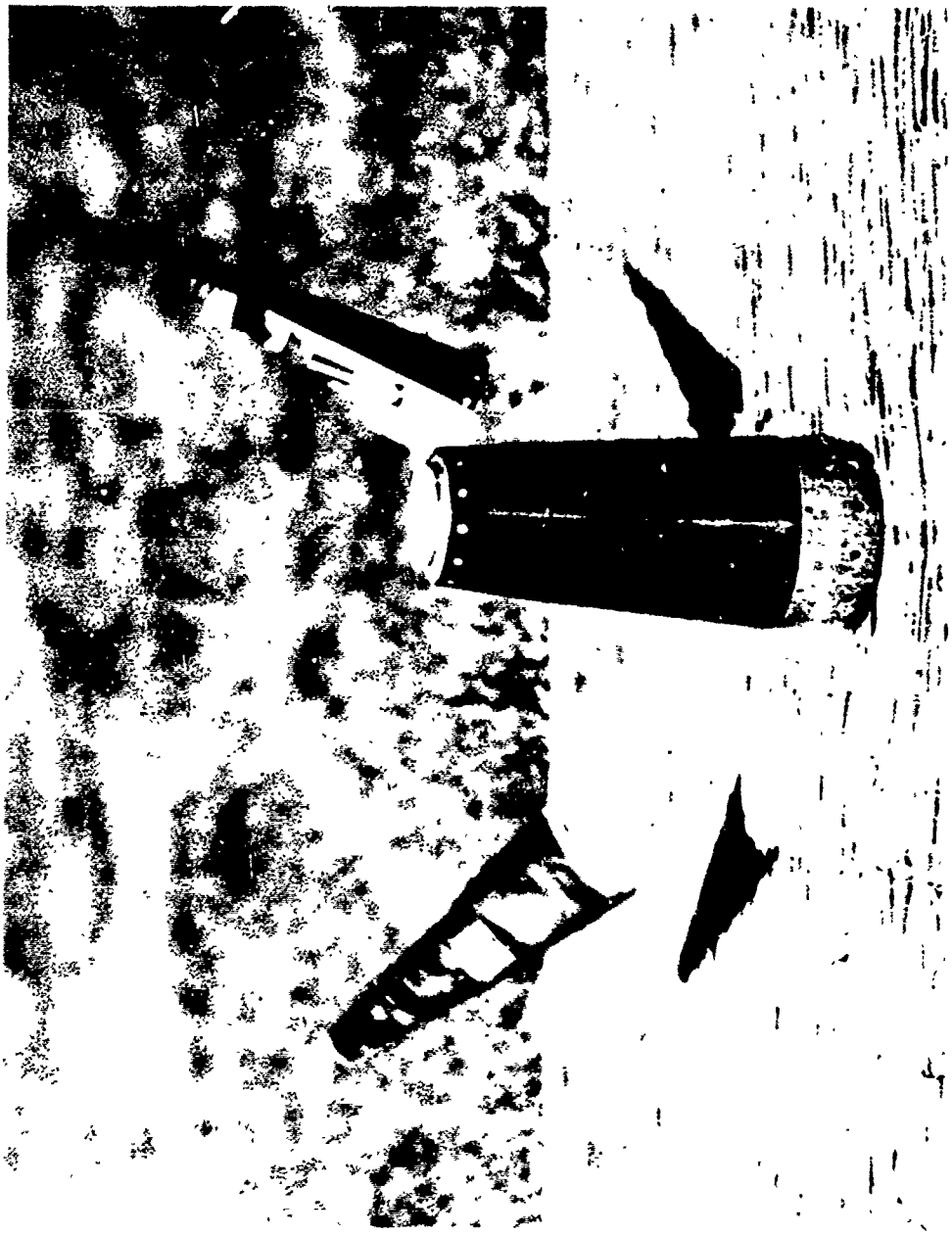

Figure 8. A photograph of an Arcas nosetip separation test showing the means by which separation is achieved.

Figure 9 is a block diagram of the electronic circuitry which controls nosetip separation. As illustrated in the block diagram, the nosetip separation circuitry is entirely independent of the remaining payload. It contains its own power supply and timing devices and the explosive device by which separation is accomplished. The circuitry is made operable by closing the arming switch which simply connects the power supply to the remaining circuitry. Indeed, this connection has no effect whatever unless the "G" switch is actuated. This closure occurs in operation at the time of rocket launch. Following closure of the "G" switch, the primary timer circuitry is activated, and after a predetermined elapsed time, an output signal is fed through the baroswitch (which closes at 75,000 ft ± 5,000 ft) to the primary guillotine firing circuit. Closure of the baroswitch starts a secondary timing circuit which provides a backup signal which fires the guillotine if the primary signal fails.

In the event that the primary timer is activated and the baroswitch has not closed, an automatic reset circuit resets the primary timer, and the system is again ready for use.

Conversely, if the rocket is launched but the primary circuit fails, closure of the baroswitch initiates the secondary timer, which will fire the guillotine and eject the nosetip.

Figure 10 is a schematic diagram of the nosetip separation electronics.

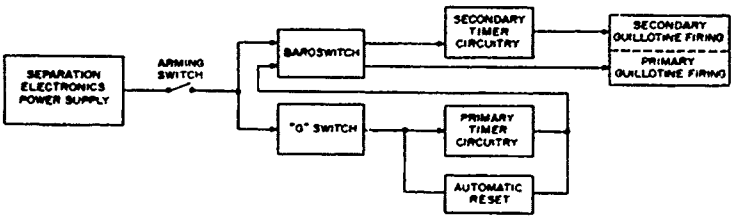

Figure 9. A block diagram of the nosetip separation circuitry.

Physically, the separable nosetip need not be of consistant size. Its length may vary and in fact does so, being dependent upon the diameter which it is required to clear. Its relationship to each payload is shown pictorially in the individual sections which follow.

No monitor of actual nosetip separation was provided on any of these devices, but separation can be detected by monitoring instrument outputs. Table III shows the primary and secondary timer settings (pre-launch) for each of the three mesospheric probes.

TABLE III

MESOSPHERIC PROBE NOSETIP SEPARATION

TIMER SETTINGS

Vehicle and Payload	Primary Timer Setting	Secondary Timer* Setting
Arcas 71-2 Lyman-Alpha and Atomic Oxygen Super Arcas	70 sec.	33 sec.
Arcas 71-3 1.27-μ Radiometer Sparrow-Arcas	63 sec.	30 sec.
Arcas 71-4 Nitric Oxide Sparrow-Arcas	53 sec.	20 sec.

*Seconds after baroswitch closure (75,000 ft ± 3,000 ft)

ARCAS 71-2, Instrumentation (O, Lyman-α Payload)

The overall relationship of the instruments aboard Arcas 71-2 is

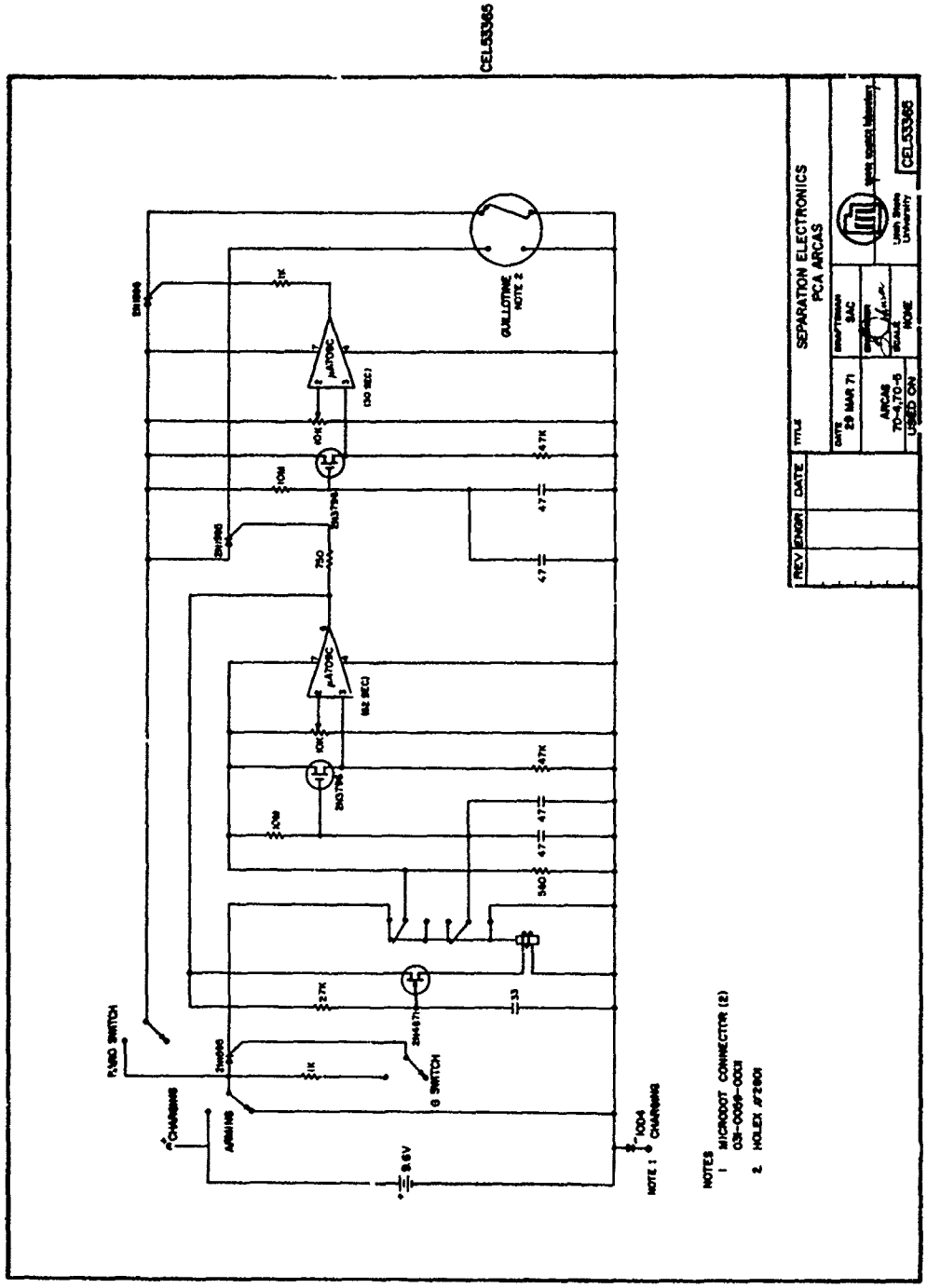

Figure 10. A schematic diagram of the nosetip separation electronic circuitry.

shown in block diagram form in Figure 11. Figure 12 is a photograph of the payload with the skin removed and shows the physical relationship of instruments within the payload.

Atomic Oxygen Detector

The basic atomic oxygen detector consists of a logarithmic ohmeter which monitors the resistance of a thin silver film. During the flight of the vehicle, after the dense portion of the atmosphere has been traversed, the silver coated sensors are exposed and, as atomic oxygen flows over the silver film, it reacts to form silver oxide which is a semiconductor. Hence, by monitoring the increasing resistance of the film, the integrated concentration of atomic oxygen can be inferred. In the Arcas 71-2 application four detection channels were used. Three of the detectors were 1 mm diameter glass rods, 1 cm in length with a vacuum deposited, 150 Å thick, silver film coating [*Thomas*, 1970; *Henderson and Schiff*, 1970]. The fourth detector was of a different configuration with a circular sensing area 2 mm in diameter. These sensors were housed in an evacuated chamber prior to nosetip separation to avoid contamination. After nosetip separation the chamber was opened and the sensors exposed. Figure 12 shows the chamber in the closed configuration, and Figures 13 and 14 show the opening and final measuring configuration.

In each channel the detectors are followed by logarithmic amplifiers which provide the channel output. The electronic circuitry for the atomic oxygen detector is shown schematically in Figure 15.

Lyman-Alpha Detector

As can be seen by reference to the block diagram of the Arcas 71-2 payload (Figure 11), the Lyman-alpha detector consists of a nitric oxide ionization chamber with a lithium fluoride window (Melpar No. CGGL 1350) and a sensitive logarithmic amplifier. The chamber is used to convert incident Lyman-alpha radiation to an electrical signal proportional in amplitude to the Lyman-alpha intensity. The amplifier logarithmic characteristics are gained from the electrometer, shown in the schematic

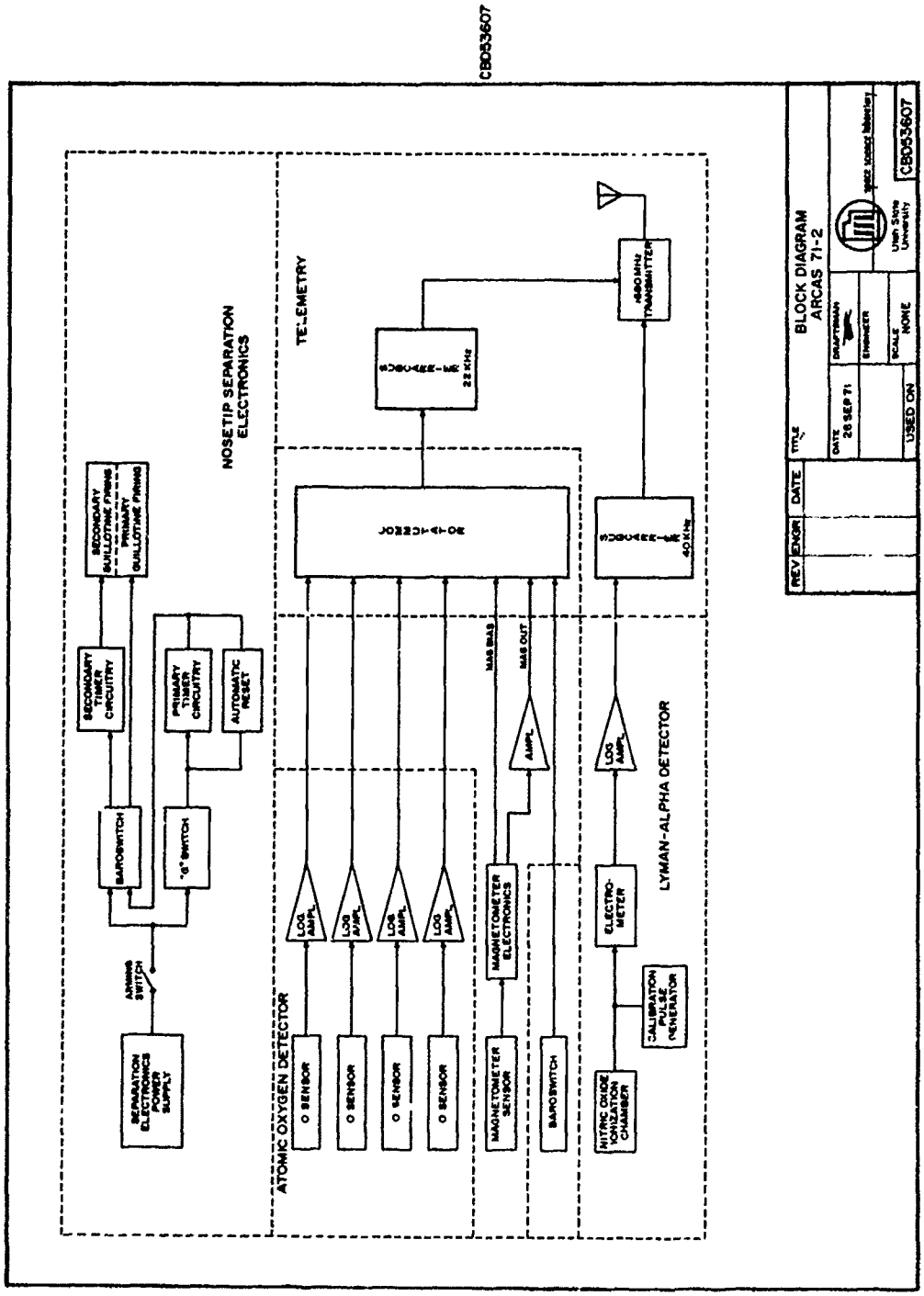

Figure 11. A block diagram of the complete Arcas 71-2 payload.

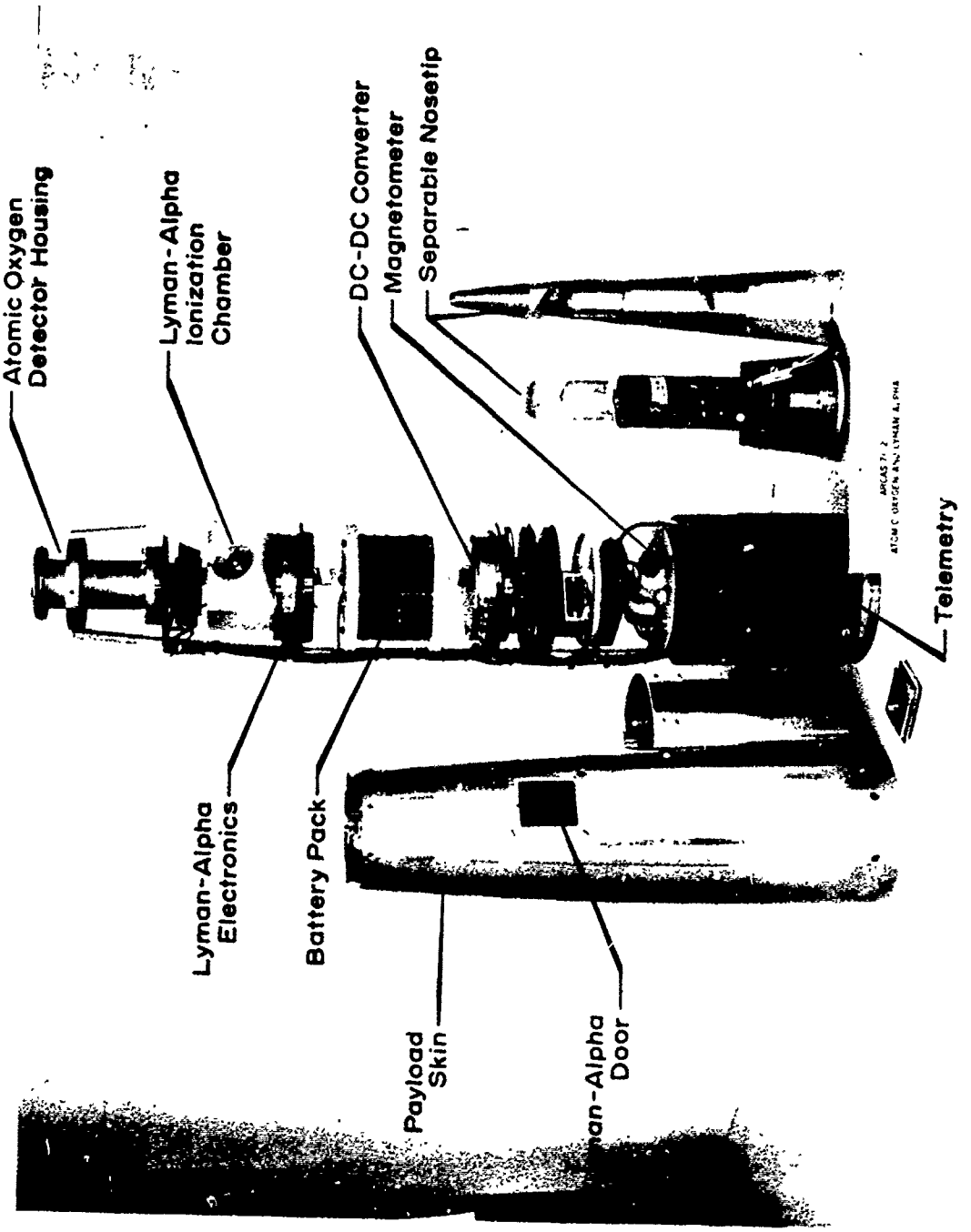

Figure 12. A labeled photograph of the Arcas 71-2 payload showing instrumentation details.

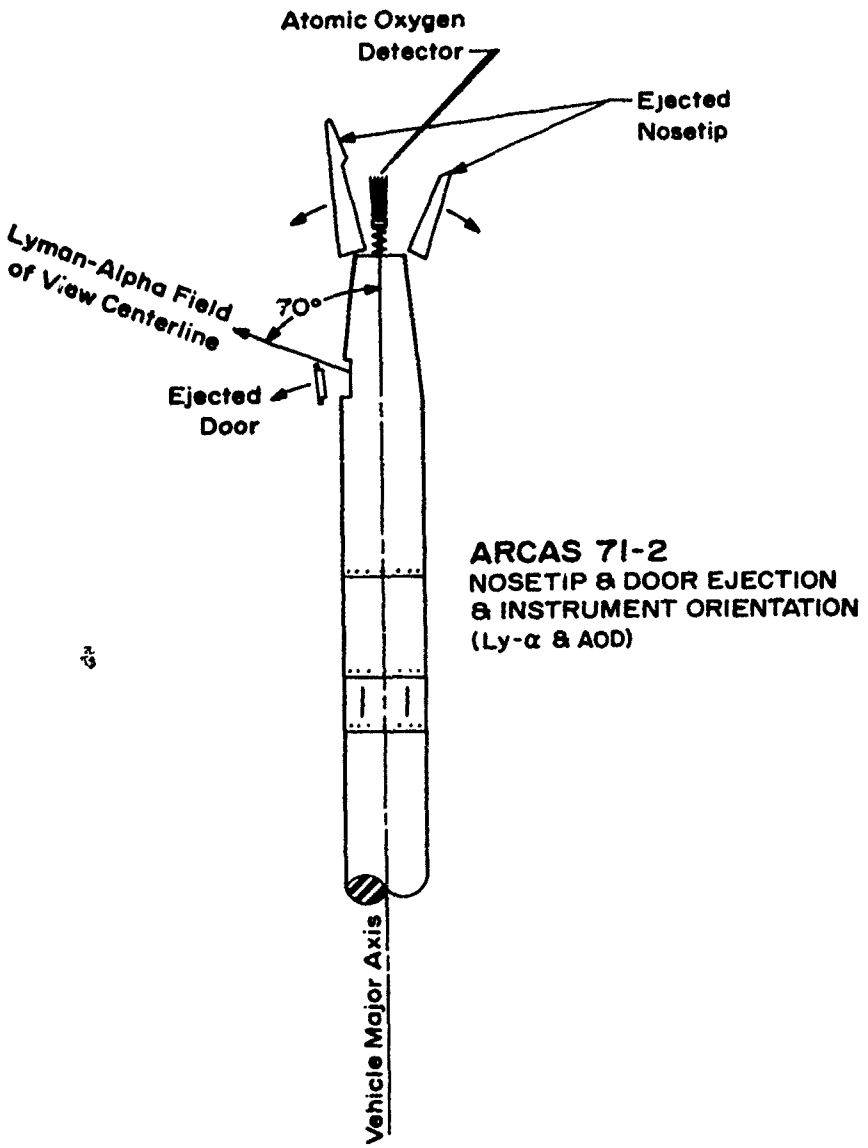

Figure 13. A schematic representation portraying the means of exposing both measuring instruments aboard Arcas 71-2.

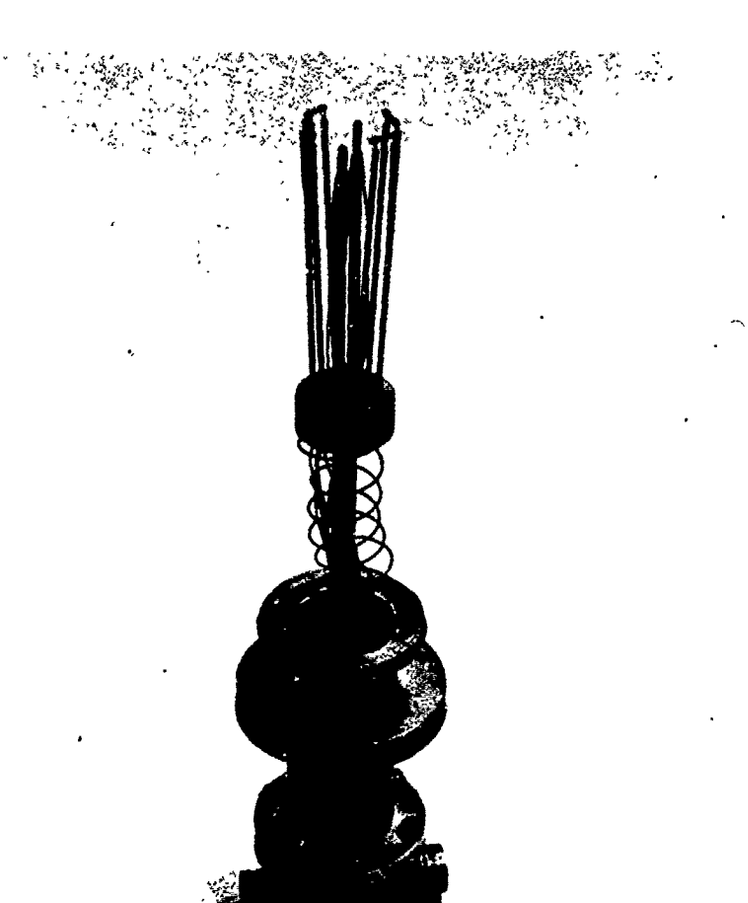

Figure 14. A photograph of the atomic oxygen sensor contained aboard Arcas 71-2.

diagram of Figure 15 by holding the plate current constant by a feedback voltage to the screen grid. The screen grid voltage required to accomplish this is the logarithmic output from the tube. This output is then properly conditioned to provide the instrument's output signal.

The instrument is also equipped with circuitry which provides a calibration pulse once approximately each 17 seconds. The pulse is obtained by momentarily (~ 20 ms) connecting the electrometer input through 1.04×10^{10} ohms to a voltage divider. This provides an instrument output pulse which serves as a check of proper instrument operation prior to and during flight.

The detector covers an energy range of from approximately 2×10^{-3} ergs cm^{-2} to 20 ergs cm^{-2}. The instrument was mounted to view with a centerline at 70° with respect to the vehicle major axis. Appendix A contains reference information and calibration for the instrument.

Support Instrumentation

Magnetometer & Baroswitch

Orientation of the magnetometer with respect to the remainder of the payload is shown in Figure 12. This device is included in the payload to provide an indication of payload orientation with respect to earth's magnetic field. Magnetometer calibrations are included in Appendix A. Baroswitch closure is at 75,000 ft ± 3,000 ft and provides a trajectory checkpoint.

16-Segment Commutator

As illustrated in the schematic diagram (Figure 14), outputs from the four-channel atomic oxygen detector, magnetometer, and baroswitch are commutated, and this commutated signal is fed to the subcarrier oscillator operating at 22 KHz. The commutator is a 16 segment device with a frame rate of 16 fps. Figure 16 is a schematic diagram of the device. Commutator segment assignments for the Arcas 71-2 payload are included in Appendix A.

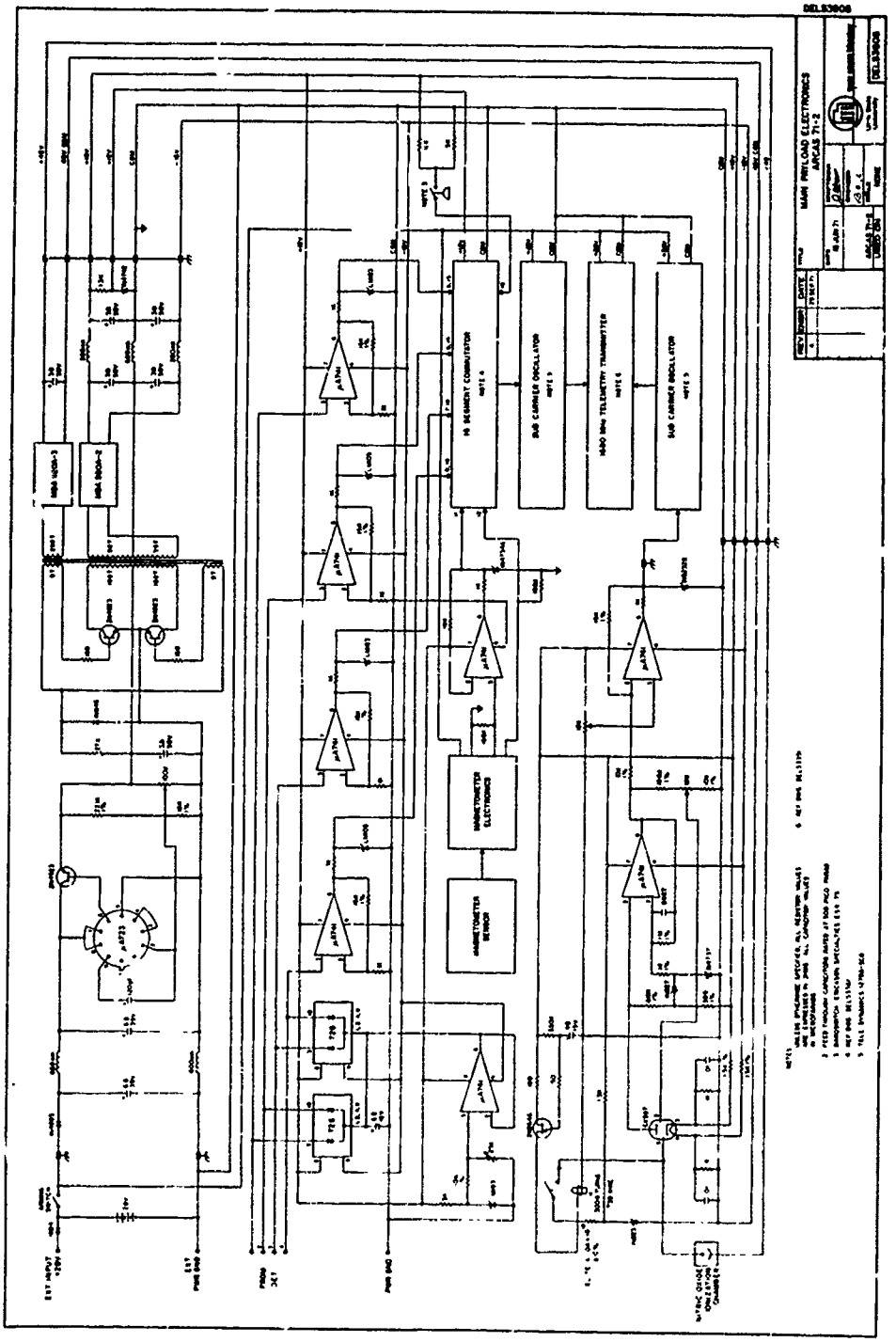

Figure 15. A schematic diagram of the Arcas 71-2 payload electronics.

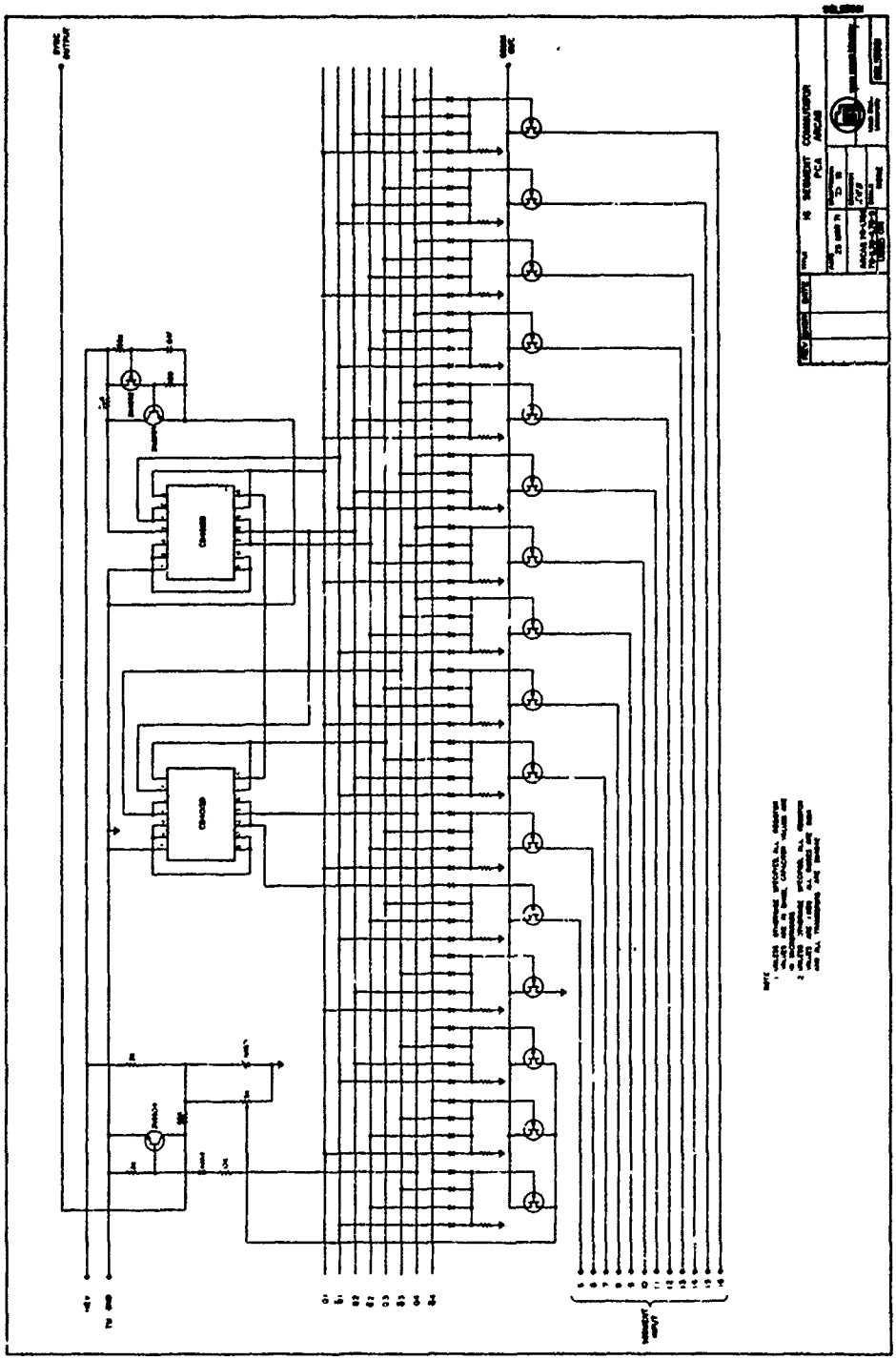

Figure 16. A schematic diagram of the 16-segment electronic commutator.

1680 MHz Telemetry Transmitter

The meteorological sites from which the Arcas rockets are launched are standardly equipped with facilities to monitor and record transmissions at 1680 MHz as this frequency has been assigned for use in meteorological work. To fully take advantage of these launch sites and their equipment the Arcas rockets are equipped with telemetry transmitters which operate at 1680 MHz. Figure 17 is a schematic diagram of the telemetry transmitter. The transmitter is FM modulated with an output power of approximately 1 watt. The signal is received and recorded at the ground station by the GMD receivers which are standard equipment at these sites.

ARCAS 71-3, Instrumentation (IR Radiometer Payload)

The physical configuration of Arcas 71-3 is described photographically in Figure 18. Figure 19 is a block diagram of the entire Arcas 71-3 payload and shows interrelationships between the instruments on that payload. Examination of the block diagram will show that the separable nosetip assembly of Arcas 71-3 included circuitry not contained in the other two Arcas configurations. This circuitry, the calibration lamp drive circuit and calibration lamp itself, were included to provide a means of monitoring the status of the 1.27-μ, cooled radiometer in the main payload during preflight and early flight (prior to nosetip separation). The calibration lamp does not illuminate continuously, but is pulsed for one second with a repetition approximately each thirty seconds. Figure 20 is the schematic diagram of the lamp and drive circuit.

When the separable nosetip is ejected, the calibration lamp and drive circuitry are also ejected as a portion of the nosetip. Nosetip separation also removes a pull cover so that the instrument sensitivity is not limited by a warm window. This cover is removed at an altitude high enough that water vapor concentration is low and frosting of the cold surface does not occur.

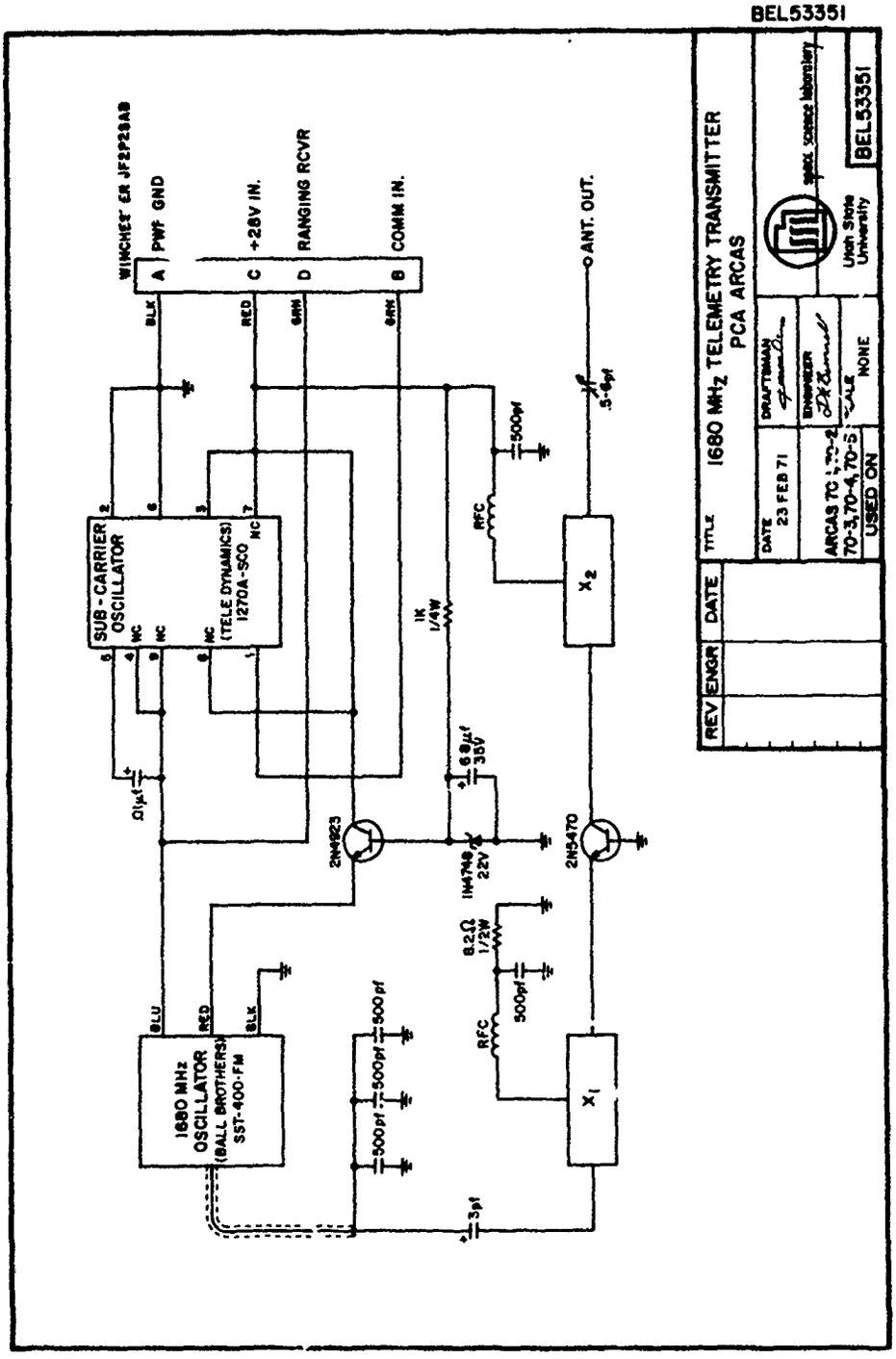

Figure 17. A schematic diagram of the 1680 MHz telemetry transmitter.

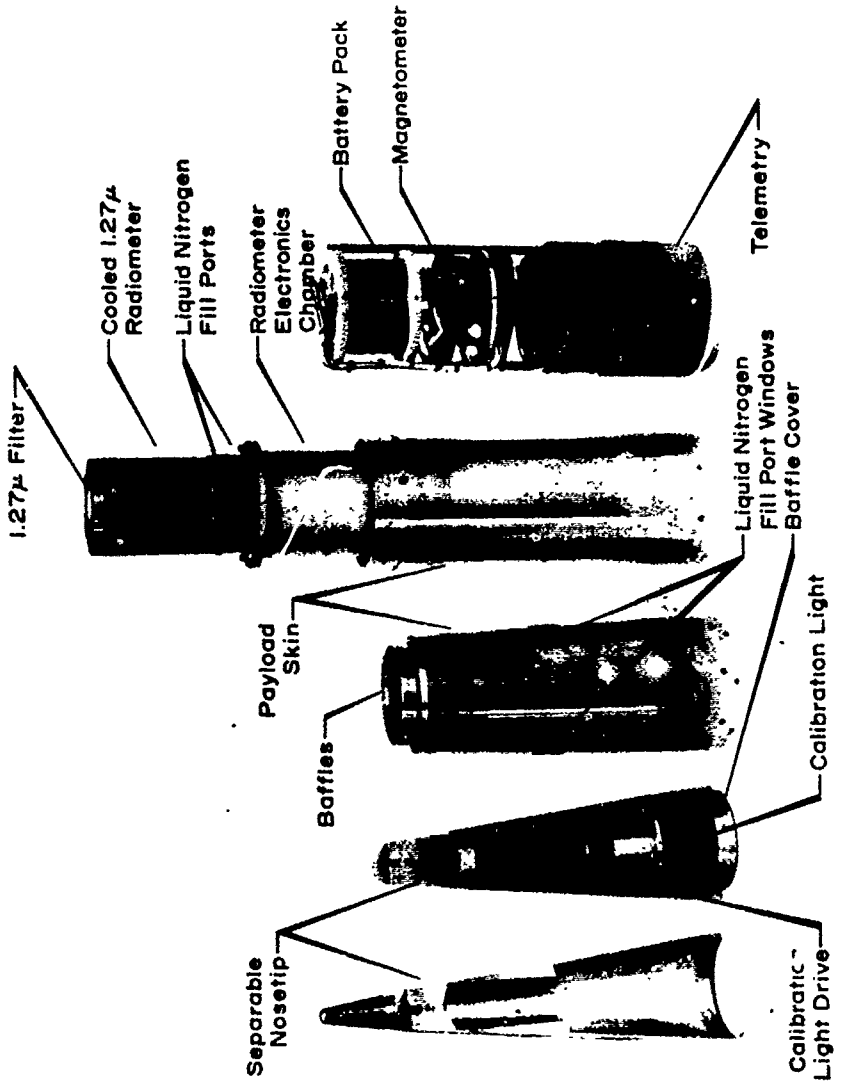

Figure 18. A labeled photograph of the Arcas 71-3 payload detailing instrument locations.

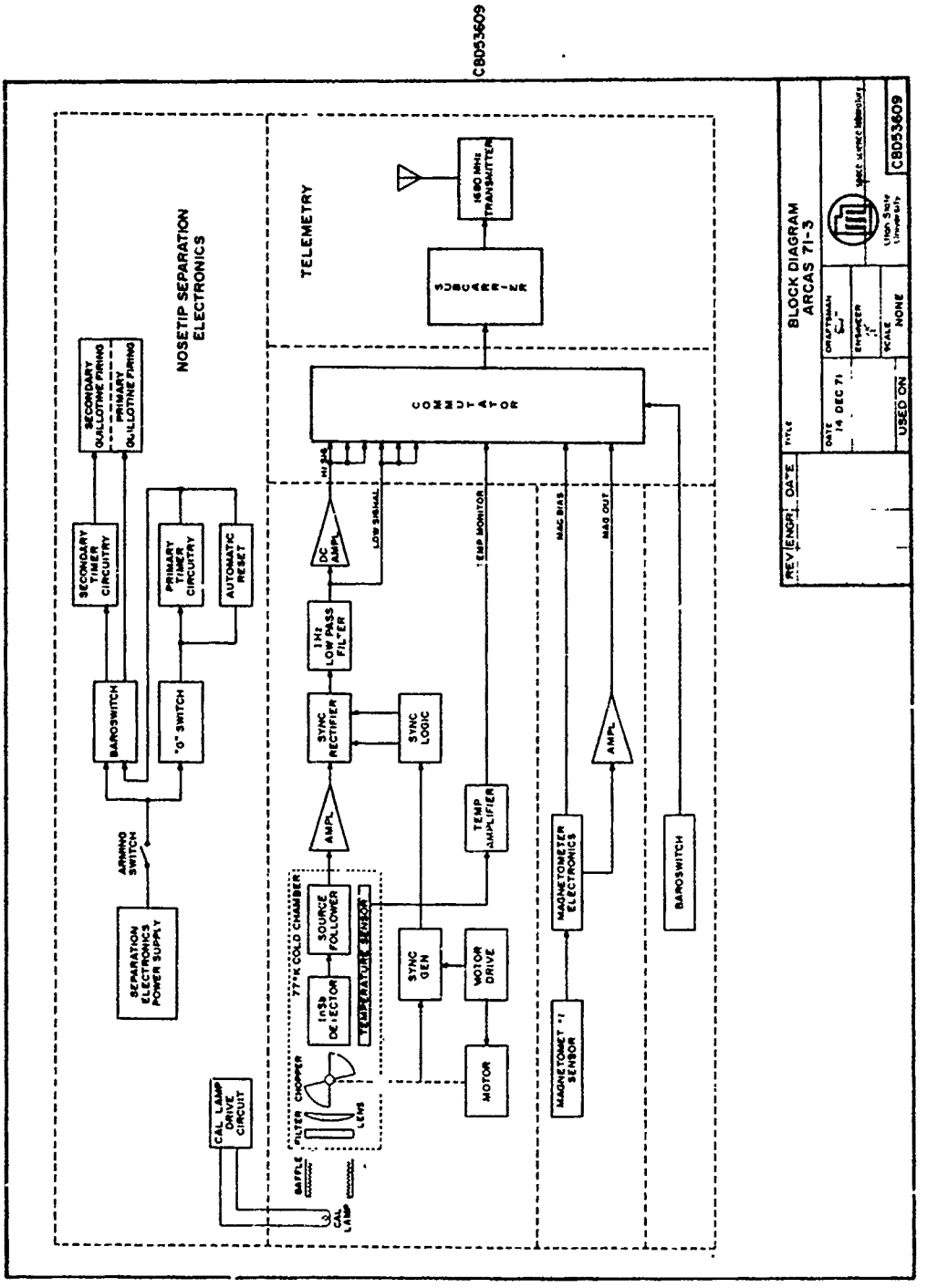

Figure 19. A block diagram of the Arcas 71-3 payload.

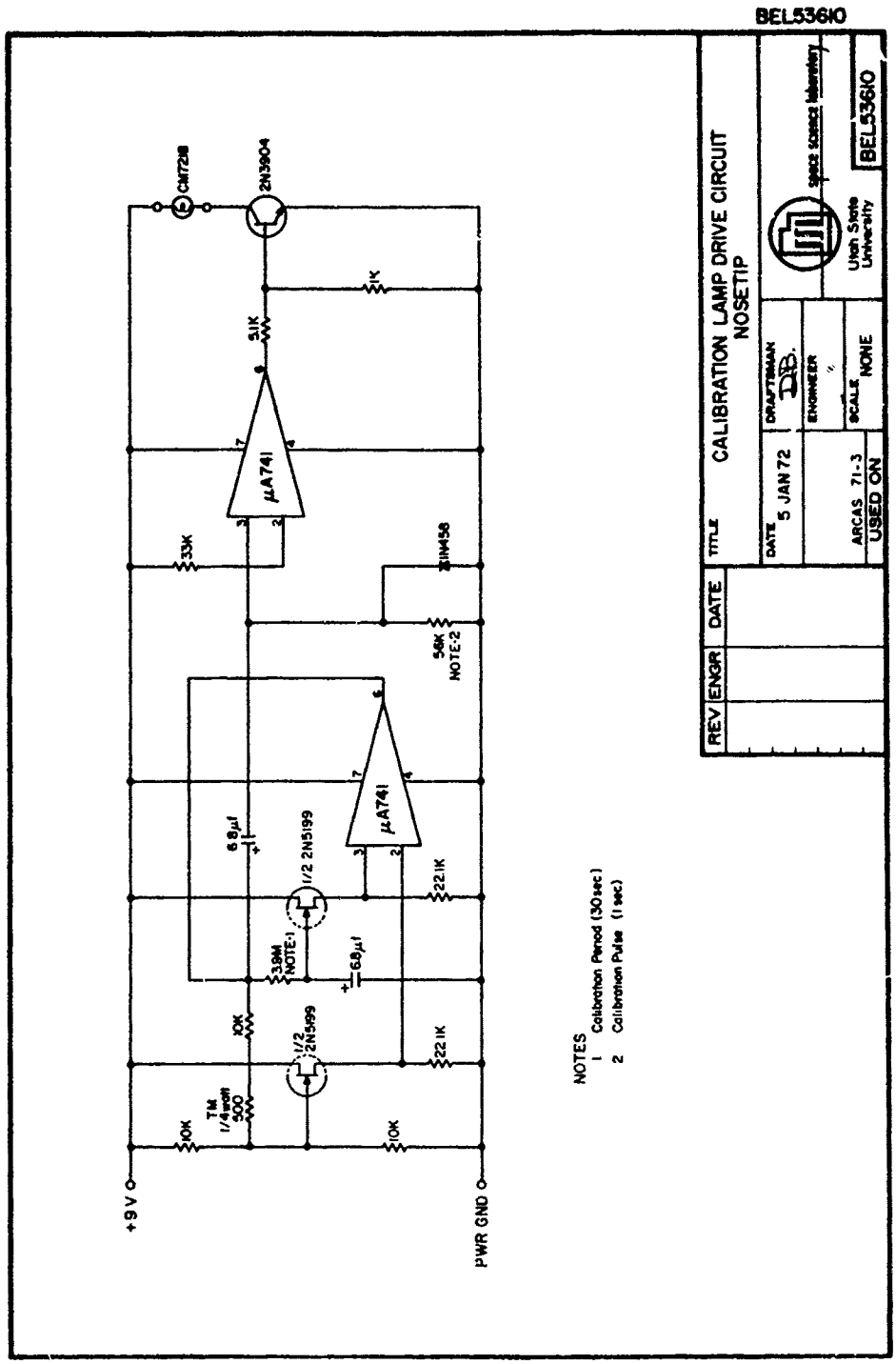

Figure 20. A schematic diagram of the 1.27-μ radiometer calibration lamp drive circuitry.

1.27-μ Radiometer

The radiometer (model NR-2) is a single channel device which is cooled with liquid nitrogen to achieve high sensitivity. Its small physical size is especially adapted to use with the Arcas rocket. The radiometer uses an Indium Antimonide (InSb) photovoltiac detector which is cooled to 77°K and has a useful range of from 1.0 to 5.5 microns. A cooled filter selects the particular wavelength and bandwidth of the radiation to be measured. In this case the filter was centered at 1.27 μ with a width to the half power points of 267 Å. The incoming signal is mechanically chopped at 266 Hz by a cooled chopper. The resulting electrical signal is amplified by a low noise amplifier with a balanced, cooled, source-follower input. This signal is synchronously rectified to produce a DC output voltage proportional to the light input. Two output channels with different gain factors are provided so that both high and low sensitivity output signals are available. The motor drive waveform and other required voltages within the radiometer are provided by the instrument itself so that only one external voltage (+28 VDC) is required by the instrument. The radiometer contains three hermetically sealed compartments. One is filled with the liquid nitrogen cryogen. A second compartment surrounds the first and is evacuated to prevent frost buildup and then backfilled with helium gas to provide heat conduction both to cool the chopper blade to the cryogen temperature and to keep the motor from becoming too hot. A sensor is provided to monitor the temperature in the cooled region.

Appendix B contains calibration and field-of-view information for the 1.27-μ cooled radiometer.

Supporting Rocketborne Instrumentation

The supporting instrumentation aboard the Arcas 71-3 payload was identical to that instrumentation contained in Arcas 71-2. Reference may be made to that section of this report for details on the commutator, transmitter, magnetometer, and baroswitch. Appendix B contains commutator segment assignments and output format and magnetometer calibration data.

ARCAS 71-4, Instrumentation (NO Photometer Payload)

The physical configuration of Arcas 71-4 is shown photographically in Figure 21. Figure 22 is a block diagram of the payload and can be used to describe the measurement technique for this particular device. The prime measurement derived from the Arcas 71-4 payload is that relating to the altitude vs. concentration profile of NO. The payload incorporates a new device, i.e., the NO γ-band photometer for obtaining this information. In operation, a photomultiplier tube alternately views atmospheric emissions through a NO-filled quartz cell and through an identical but evacuated cell. Both cells are preceded by an interference filter centered at 2155 Å, a honeycomb collimator, and a baffle assembly. The alternate viewing is accomplished by physically placing one cell and then the other in front of the photomultiplier tube. Movement of the cells is accomplished by a motor drive unit. Transit time requires approximately 0.1 sec., then the cells are in position for approximately 0.9 sec. before the sequence repeats. The NO-filled cell effectively absorbs the 2155 Å flux due to resonance fluorescence scattering by atmospheric NO and passes other wavelengths. The evacuated cell passes these same wavelengths but including the NO signal. The photometer output, therefore, alternately is due to total atmospheric scattered light passed by the interference filter, and in the second case total emissions passed by the filter minus the NO-γ band signal (absorbed by the NO filled cell). The output of the photomultiplier is amplified, converted from analog to digital form and fed to the vehicle commutator. Figure 23 is a schematic diagram of the payload.

The amplifier which follows the photomultiplier tube does not have a constant gain factor but uses the summation of three cascaded saturating amplifiers to provide data compression which can be described by simple mathematical functions over three ranges. Complete details pertaining to amplifier response and gains are included in Appendix C.

The output signals from the photomultiplier amplifier are fed to the A-D converter. This unit provides an eight-bit digital output in binary form to the commutator. Appendix C also details the format of A-D conversion.

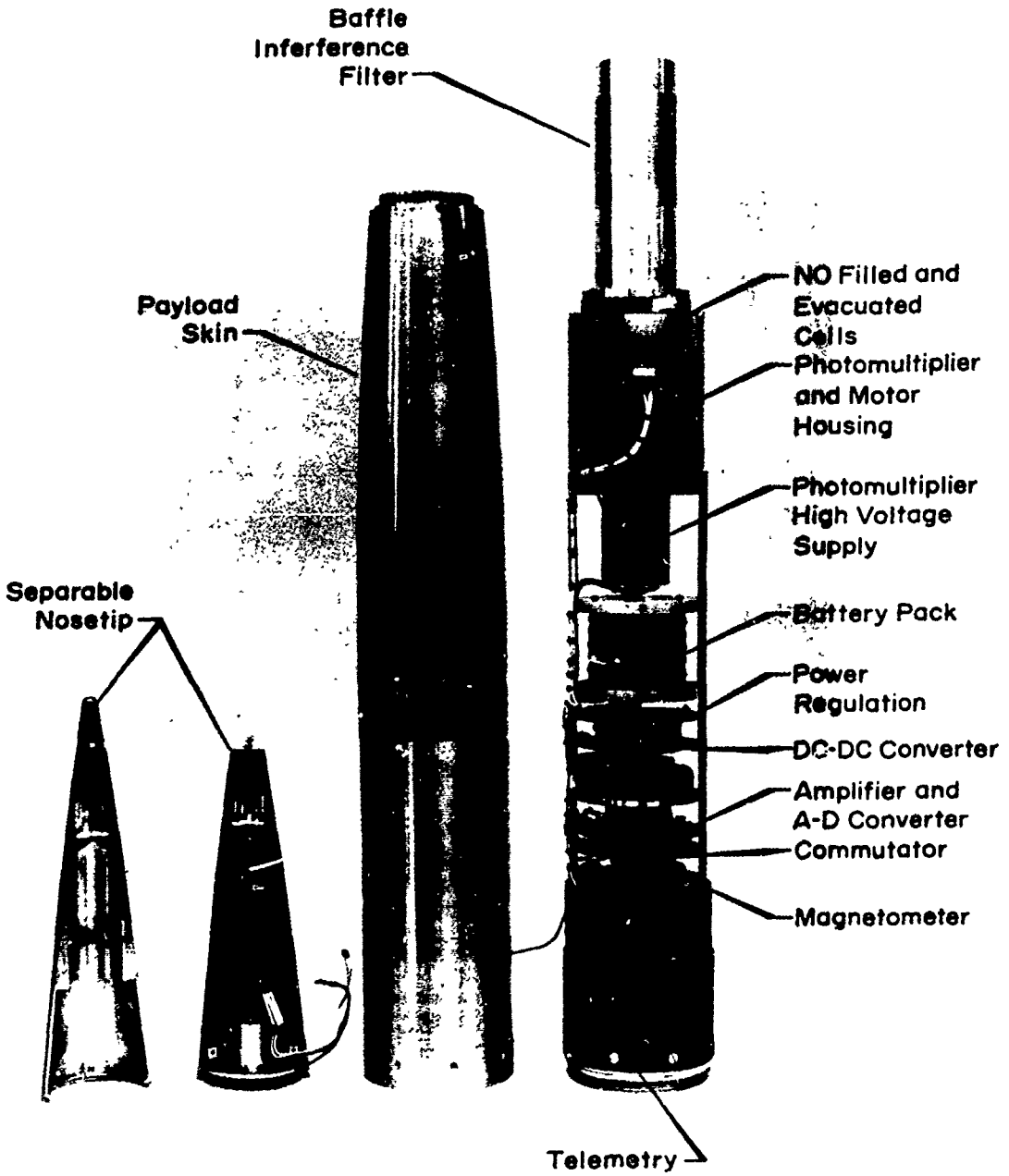

Figure 21. A labeled photograph of the Arcas 71-4 payload detailing instrument locations.

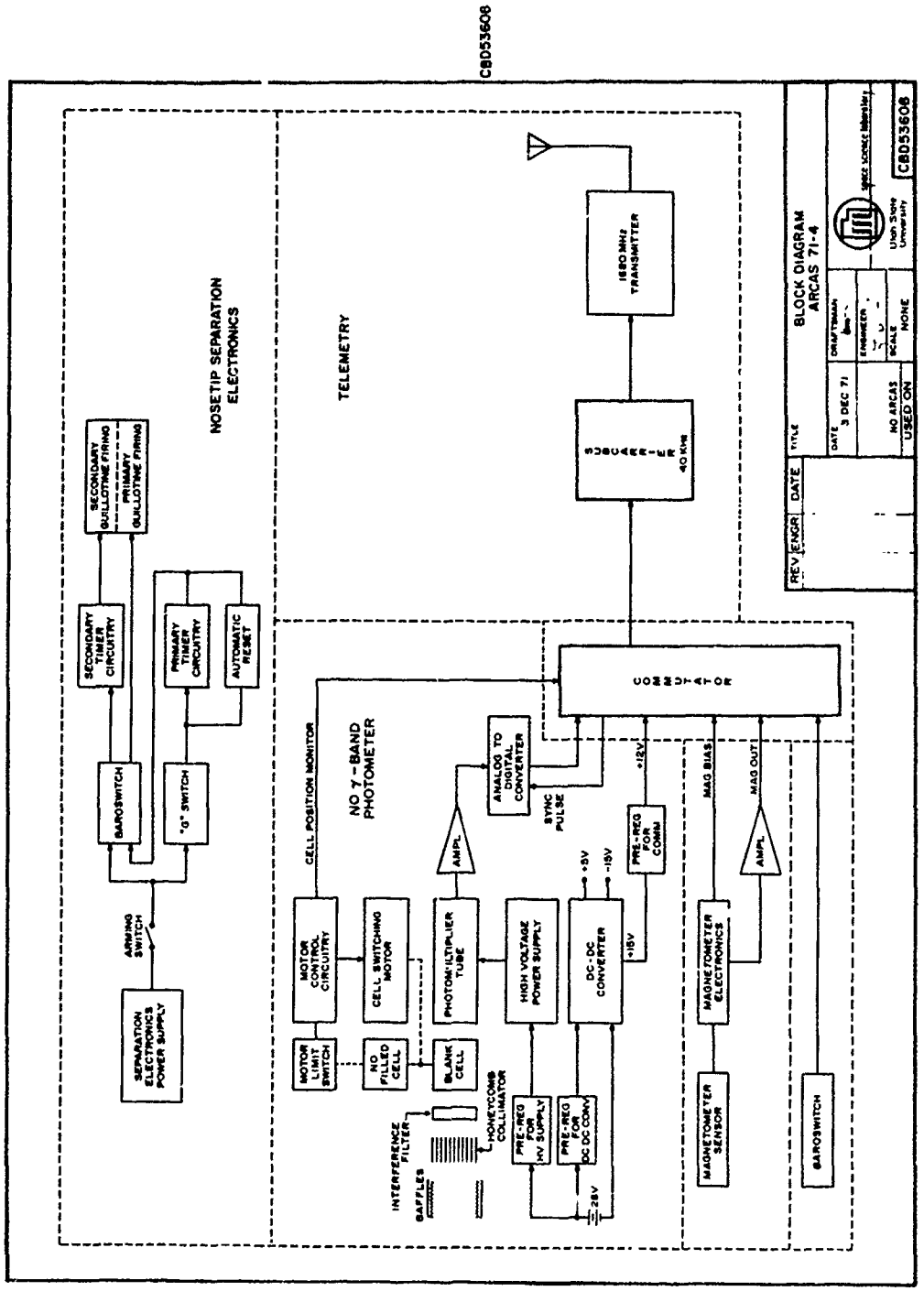

Figure 22. A block diagram of the Arcas 71-4 payload.

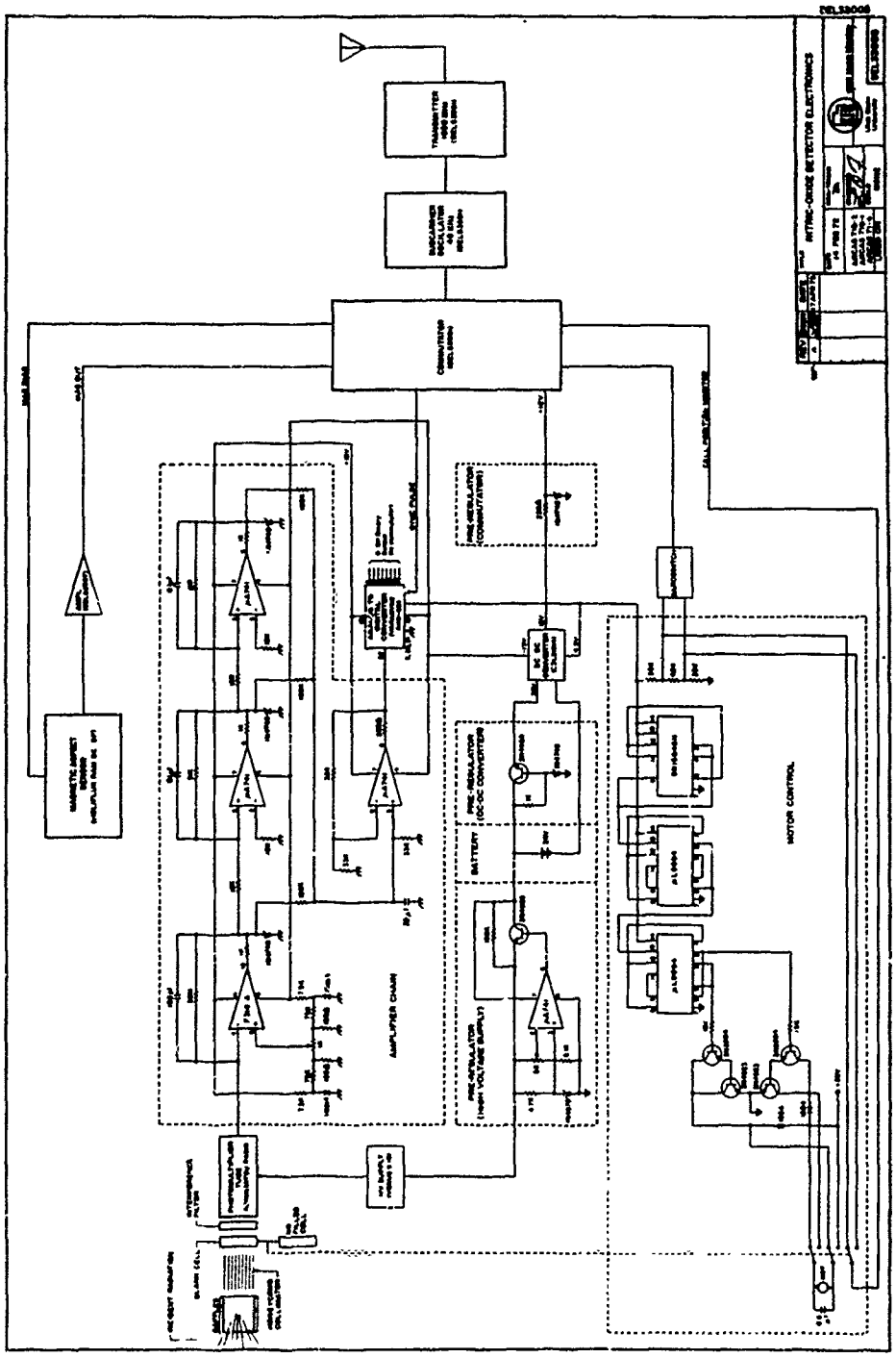

Figure 23. A schematic diagram of the Arcas 71-4 payload electronic circuitry.

Support Instrumentation

The magnetometer, baroswitch, commutator, and 1680 MHz transmitter sections of this payload were identical with those sections of Arcas 71-2. These instruments are illustrated schematically in Figures 15, 15, 16, and 17, respectively. Assignments and calibrations are included in Appendix C.

SUMMARY AND RESULTS

In reviewing the results of the mesospheric probes program it is important that the primary objective of the program be kept firmly in mind. This objective was to test fly new instruments which had been designed for probing the mesosphere. Acquisition of actual geophysical data, while desirable, was relegated to importance of a secondary nature. It is accepted without question by atmospheric investigators that laboratory tests of new instruments are a fundamental part of developing these devices, but such new devices must be utilized in actual *in situ* circumstances before their validity can be realistically analyzed. Often, repeated attempts must be made before a new device and a technique can be successfully evaluated, with each attempt serving as a further step in developing a useful device.

The primary objective of test flying each of the new instruments was accomplished during the mesospheric probes program. Data accumulation, although restricted and not sufficient for a thorough analysis of mesospheric conditions, was extremely significant for the purposes of probe analysis. A brief summary of the results of each flight is included below.

Arcas 71-2

This payload reached an apogee of 106 km at launch +100 sec. The instrument experienced bad telemetry signal, fading after approximately launch +90 sec. An indication of successful atomic oxygen and Lyman-alpha measurements was obtained, however, for a brief period prior to telemetry fadeout. Indications are that the weak signal was due to

ground station malady rather than instrument failure, and that the payload functioned properly although the oxygen sensor probably was not as sensitive as desired.

Arcas 71-3

This instrument for measuring 1.27-μ radiation from $O_2(^1\Delta_g)$ reached an apogee of 130 km at launch +185 sec. The payload experienced a sudden loss of telemetry at launch +86 sec. Prior to this signal loss the instrument indicated a short period of what appeared as probably normal signal. Some unexpectedly high signals were present at earlier times and were probably due to nosetip heating prior to ejection and viewing of the hot nosetip for a period subsequent to ejection. These signals are obviously from sources other than atmospheric emissions as evidenced by their magnitude. The flight of this instrument was extremely significant in that through its use in the mesospheric probes program, development was placed at a level such that succeeding instruments could be utilized in an auroral program conducted at Fairbanks, Alaska, in early 1972. The succeeding instruments were extremely successful.

Arcas 71-4

This payload, which was designed to measure nitric oxide concentrations, reached an apogee of 137 km at launch +185 sec. It provided output (TM) signals throughout the flight, but the output of the device was at an unexpectedly high level and reached saturation levels periodically during the flight. It is believed that this situation resulted from high voltage corona at the face of the photomultiplier tube. The periods of saturation corresponded to the payload coning rate (10 seconds out of each 30 seconds) and occurred when the instrument was most nearly pointed in the solar direction. It is thought that the high signal levels due to corona and the additional signals due to sunlight (when the payload pointed in that direction) were responsible for the periods of saturation.

Subsequent investigations indicated that the corona was indeed a likely suspect, and succeeding instruments have been designed to preclude

the possibility of this condition. Although this flight did not provide data suitable for analysis of mesospheric conditions per se, it did prove the major system to be flight worthy although pointing out significant areas of required instrument redesign.

REFERENCES

Barth, C. A., Rocket measurement of the nitric-oxide dayglow, *J. Geophys. Res.*, *69*, 3301, 1964.

Barth, C. A., Rocket measurements of nitric oxide in the upper atmosphere, *Planetary Space Sci.*, *14*, 623, 1966.

Ferguson, E. E. and F. C. Fehsenfeld, Thermal energy reactions of C- with O_2, N_2O, CO and CO_2, *J. Chem. Phys.*, *53*, 2614, 1970.

Gattinger, R. L., *The Radiating Atmosphere*, 258, Reidel Publishing Co., Dordrecht, Holland, 1971.

Henderson, W. R. and H. I. Schiff, A simple sensor for the measurement of atomic oxygen height profiles in the upper atmosphere, *Planetary Space Sci.*, *18*, 1527, 1970.

Huffman, R. E., D. E. Paulson, J. C. Larabee, and R. B. Cairns, Decrease in D-region $O_2(^1\Delta_g)$ photoionization rates resulting from CO_2 absorption, *J. Geophys. Res.*, *76*, 1028, 1971.

Hunt, B. G., Photochemistry of ozone in a moist atmosphere, *J. Geophys. Res.*, *71*, 1385, 1966.

Hunten, D. M. and M. B. McElroy, Metastable $O_2(^1\Delta)$ as a major source of ions in the D-region, *J. Geophys. Res.*, *73*, 2421, 1968.

Megill, L. R., A. M. Despain, D. J. Baker and K. D. Baker, Oxygen atmospheric and infrared atmospheric bands in the aurora, *J. Geophys. Res.*, *75*, 4775, 1970.

Meira, L. G. Jr., Rocket measurements of upper atmospheric nitric oxide and their consequences to the lower ionosphere, *J. Geophys. Res.*, *76*, 202, 1971.

Noxon, J. F., Auroral emission from $O_2(^1\Delta_g)$, *J. Geophys. Res.*, *75*, 1879, 1970.

Pearce, J. B., Nitric oxide gamma-band emission rate factor, *J. Quantitive Spectroscopy and Radiative Transfer*, *9*, 1593, 1969.

Thomas, R. J., A silver oxide detector for the direct measurement of atmospheric atomic oxygen, unpublished Ph.D. thesis, Utah State University, Logan, 1970.

APPENDIX A

ARCAS 71-2

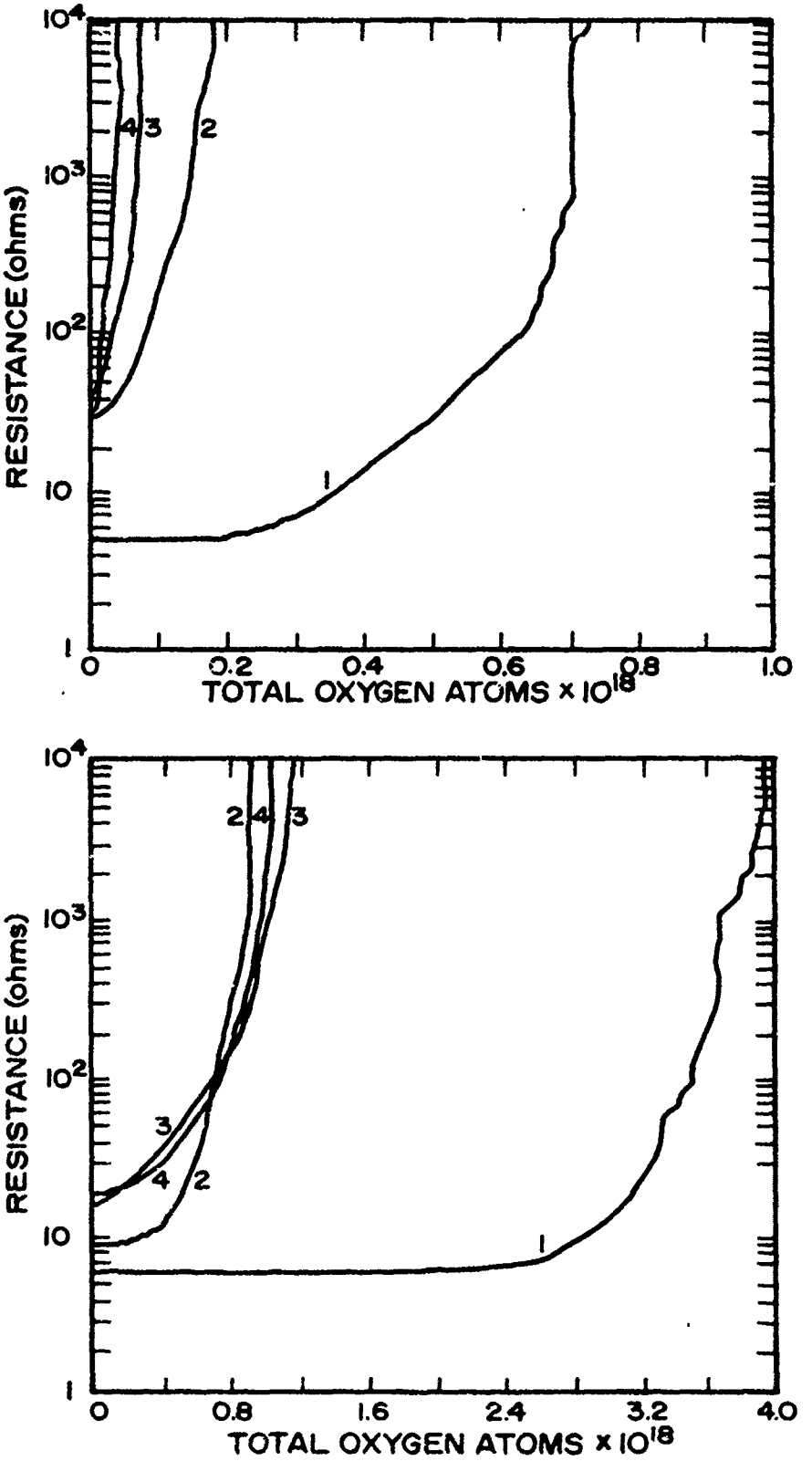

Figure A-1. Typical atomic oxygen sensor reaction curves showing initial and recycled responses.

TABLE A-1

ATOMIC OXYGEN DETECTOR

PREFLIGHT SENSOR RESISTANCES

Channel	Sensor Resistance
1	5.5 Ω
2	4.8 Ω
3	7.0 Ω
4	5.5 Ω

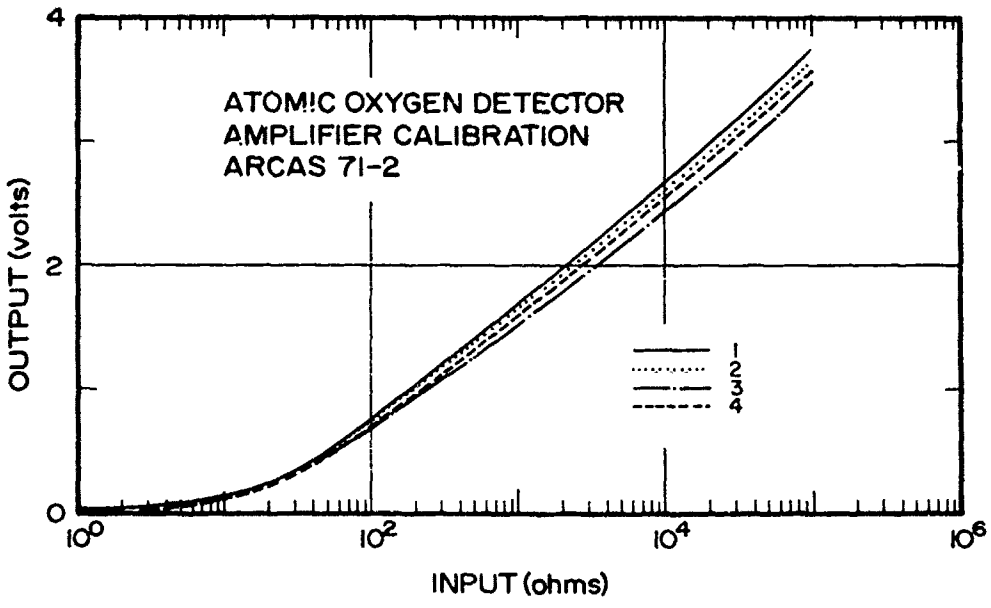

Figure A-2. Atomic oxygen detector amplifier calibration curves, Arcas 71-2.

TABLE A-2

ARCAS 71-2 LYMAN-ALPHA

CHARACTERISTICS

Field of View	45°
Aperture Area	.066 cm^2
Geometric Factor	.0316 cm^2 ster
Chamber Quantum Efficiency	24.2%
Chamber Number	M2598

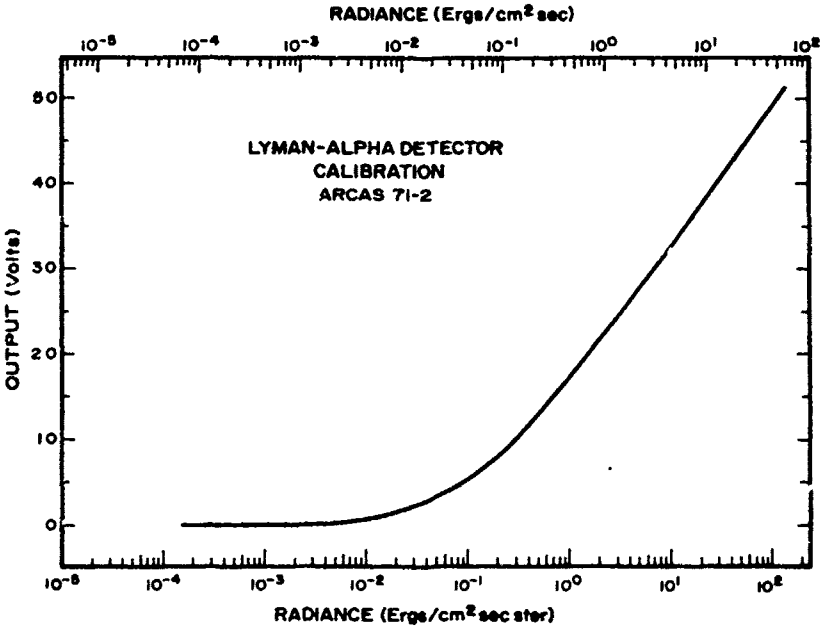

Figure A-3. Lyman-alpha detector calibration curve, Arcas 71-2.

TABLE A-3

MAGNETOMETER S/N 3369 CALIBRATION

ARCAS 71-2

Field (Milligauss)	Output (volts)	
600	4.78	
550	4.59	
500	4.39	
450	4.20	
400	4.00	
350	3.80	
300	3.60	
250	3.40	
200	3.20	
150	3.00	
100	2.80	
50	2.60	
0	2.40	(BIAS LEVEL)
-50	2.20	
-100	2.00	
-150	1.80	
-200	1.60	
-250	1.40	
-300	1.20	
-350	1.00	
-400	0.79	
-450	0.59	
-500	0.39	
-550	0.20	
-600	0.00	

Direction of Magnetic Field for voltage signals above bias level.

TABLE A-4

16 SEGMENT COMMUTATOR ASSIGNMENTS

ARCAS 71-2

Channel	Assignment
1	+5v
2	+5v
3	+5v
4	0v
5	#1 0 Detector
6	#2 0 Detector
7	#3 0 Detector
8	#4 0 Detector
9	#1 0 Detector
10	Baroswitch
11	Magnetometer Output
12	Magnetometer Bias
13	#1 0 Detector
14	#2 0 Detector
15	#3 0 Detector
16	#4 0 Detector

Commutator frame rate = 16 frames per second

Baroswitch closure at 75,000 ft ± 3,000 ft

Altitudes < 75,000 ft = 0 volts

Altitudes > 75,000 ft = +5 volts

Subcarrier Oscillators 22 KHz and 40 KHz

Telemetry Transmitter Output 1680 MHz

APPENDIX B

ARCAS 71-3

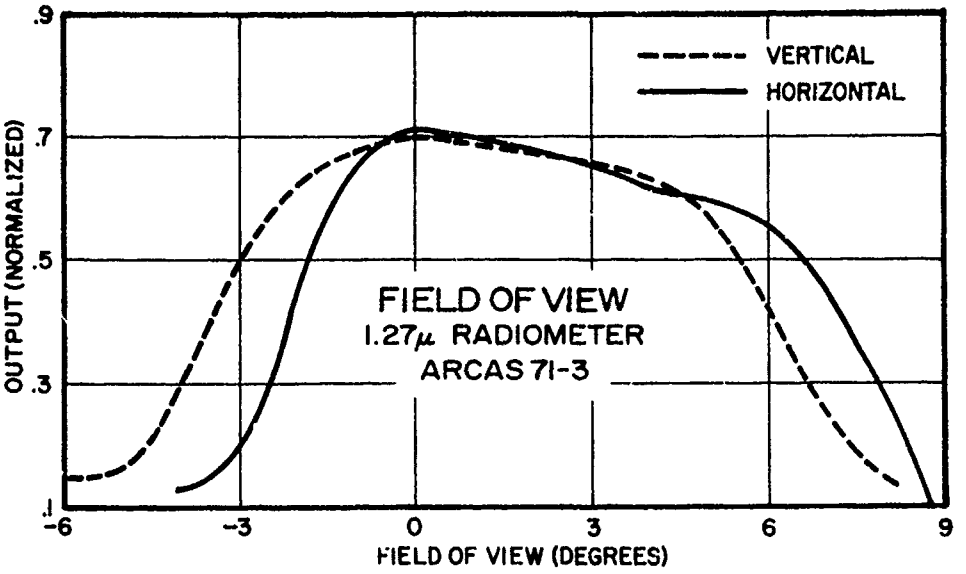

Figure B-1. 1.27-μ radiometer field of view, Arcas 71-3.

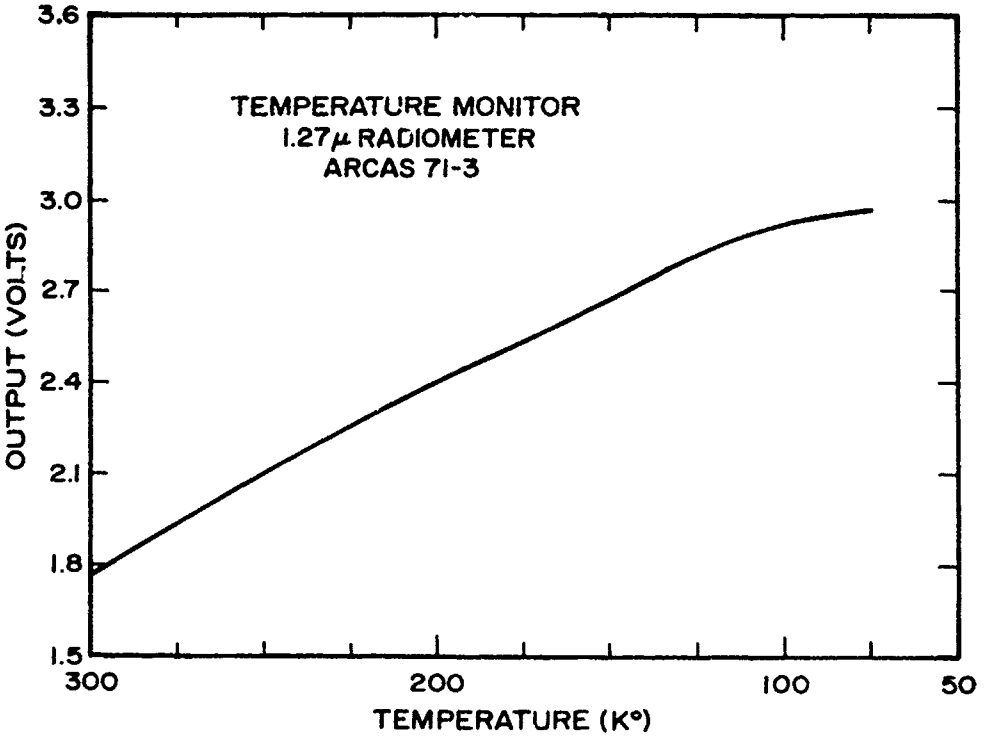

Figure B-2. 1.27-μ radiometer temperature monitor calibration, Arcas 71-3.

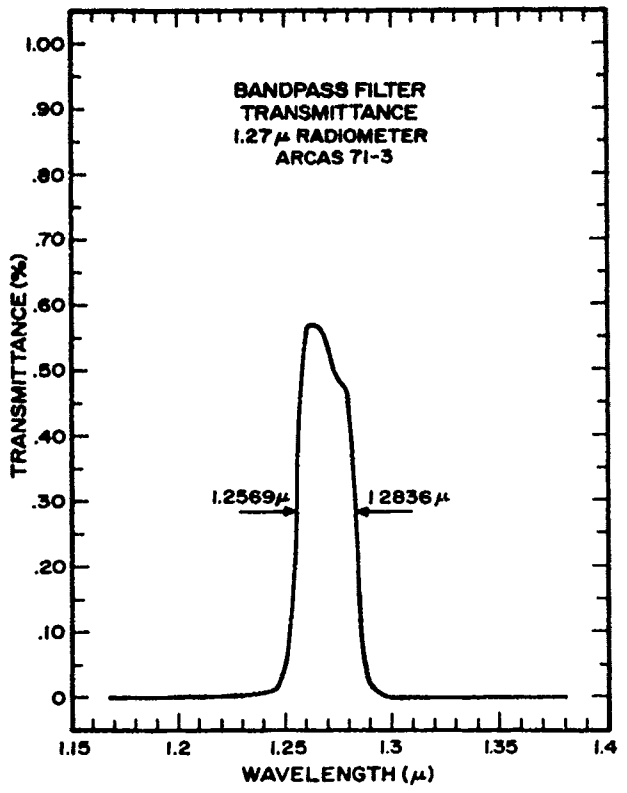

Figure B-3. 1.27-μ radiometer bandpass filter characteristics, Arcas 71-3.

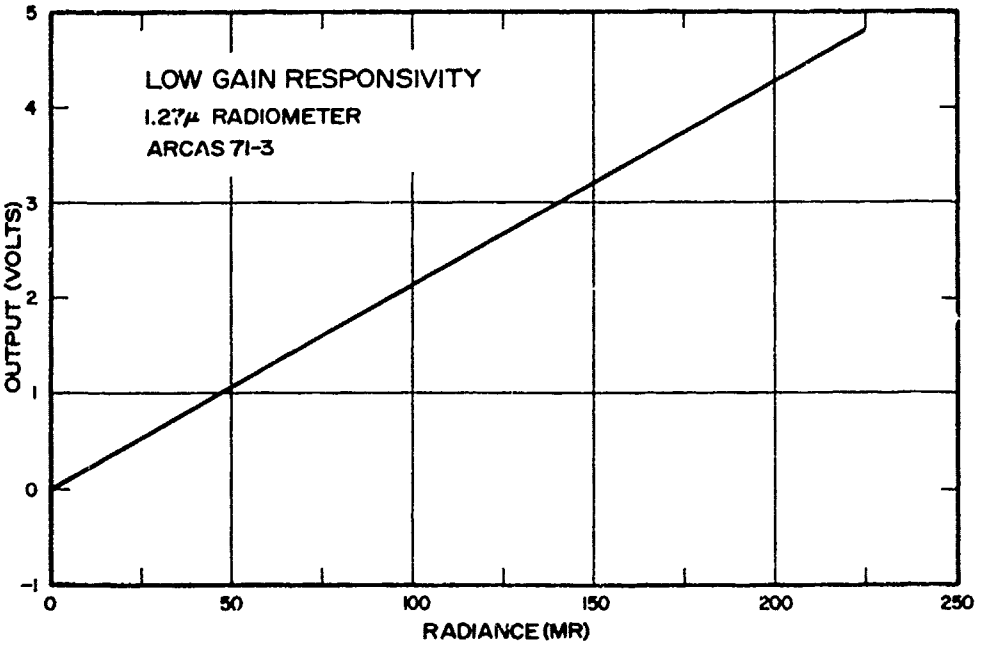

Figure B-4. 1.27-μ radiometer low gain responsivity calibration, Arcas 71-3.

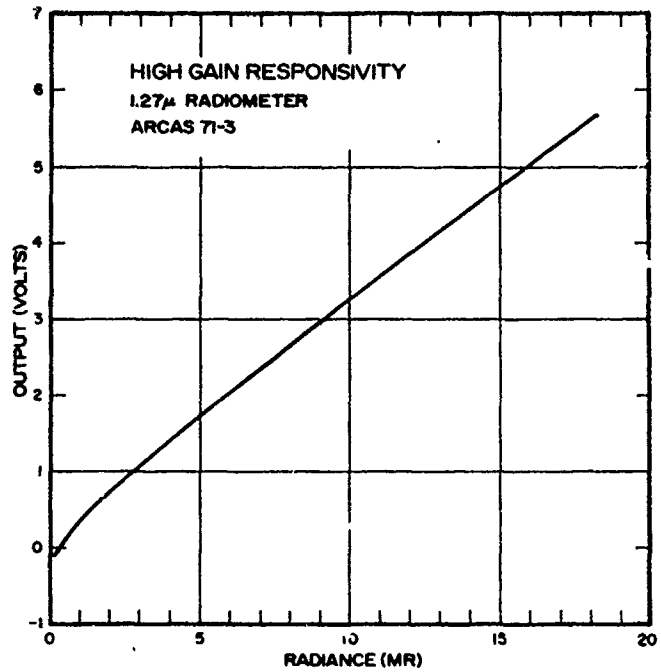

Figure B-5. 1.27-μ radiometer high gain responsivity calibration, Arcas 71-3.

TABLE B-1

MAGNETOMETER S/N 3375 CALIBRATION

Field (Milligauss)	Output (Volts)	Field (Milligauss)	Output (Volts)	Field (Milligauss)	Output (Volts)
600	4.76	200	3.19	-200	1.59
550	4.57	150	2.99	-250	1.39
500	4.38	100	2.79	-300	1.19
450	4.18	50	2.59	-350	0.98
400	3.99	BIAS LEVEL→ 0	2.39	-400	0.78
350	3.79	-50	2.19	-450	0.58
300	3.59	-100	1.99	-500	0.38
250	3.39	-150	1.79	-550	0.19
				-600	0.01

Orientation with respect to output same as shown on page A-4.

TABLE B-2

16 SEGMENT COMMUTATOR ASSIGNMENTS

ARCAS 71-3

Segment	Assignment
1	+5v
2	+5v
3	+5v
4	0v
5	Magnetometer Output
6	1.27 μ High Signal
7	1.27 μ Low Signal
8	Temperature Monitor
9	1.27 μ Low Signal
10	Baroswitch
11	1.27 μ High Signal
12	1.27 μ Low Signal
13	Magnetometer Output
14	Magnetometer Bias
15	1.27 μ High Signal
16	1.27 Low Signal

Commutator frame rate = 16 frames per second

*Baroswitch closure at 75,000 ft ± 3,000 ft

Altitudes $\leq$ 75,000 ft = 0 volts

Altitudes $\geq$ 75,000 ft = +5 volts

Subcarrier Oscillator 40 KHz

Telemetry Transmitter Output 1680 MHz

APPENDIX C

ARCAS 71-4

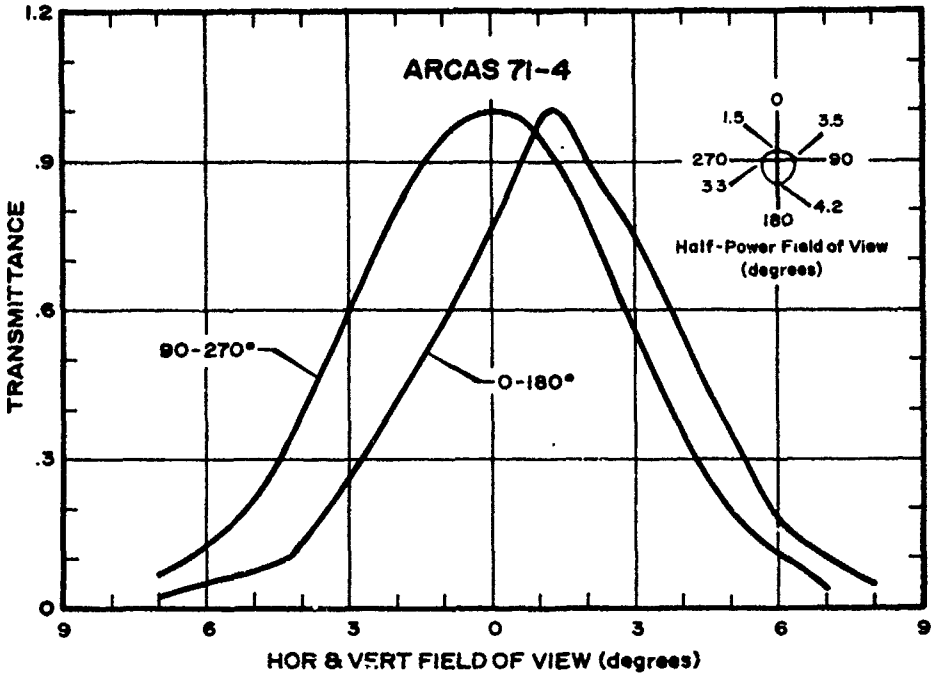

Figure C-1. Nitric oxide detector rield of view, Arcas 71-4.

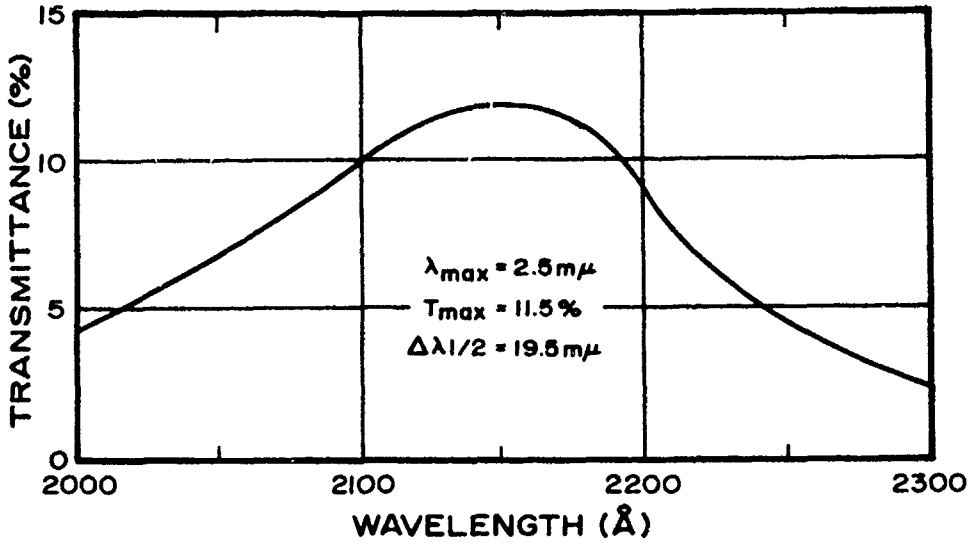

Figure C-2. Nitric oxide detector filter characteristics, Arcas 71-4.

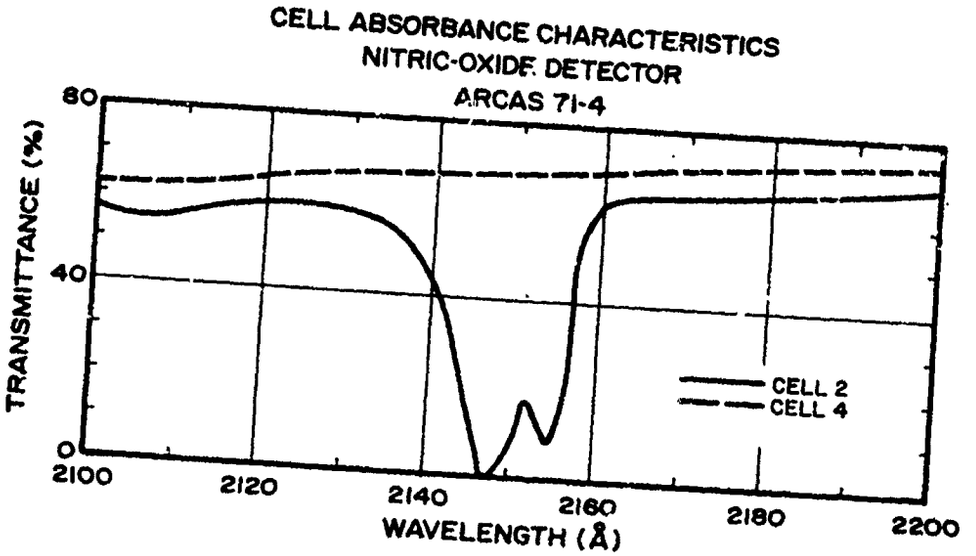

Figure C-3. Nitric oxide detector cell absorbance characteristics, Arcas 71-4. The dashed line represents the evacuated cell and the solid line the NO filled cell.

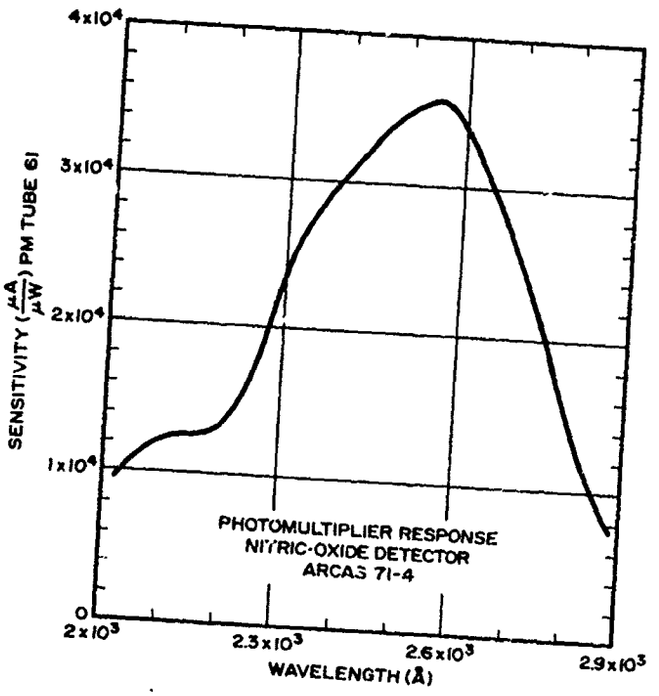

Figure C-4. Nitric oxide detector photomultiplier tube response, Arcas 71-4.

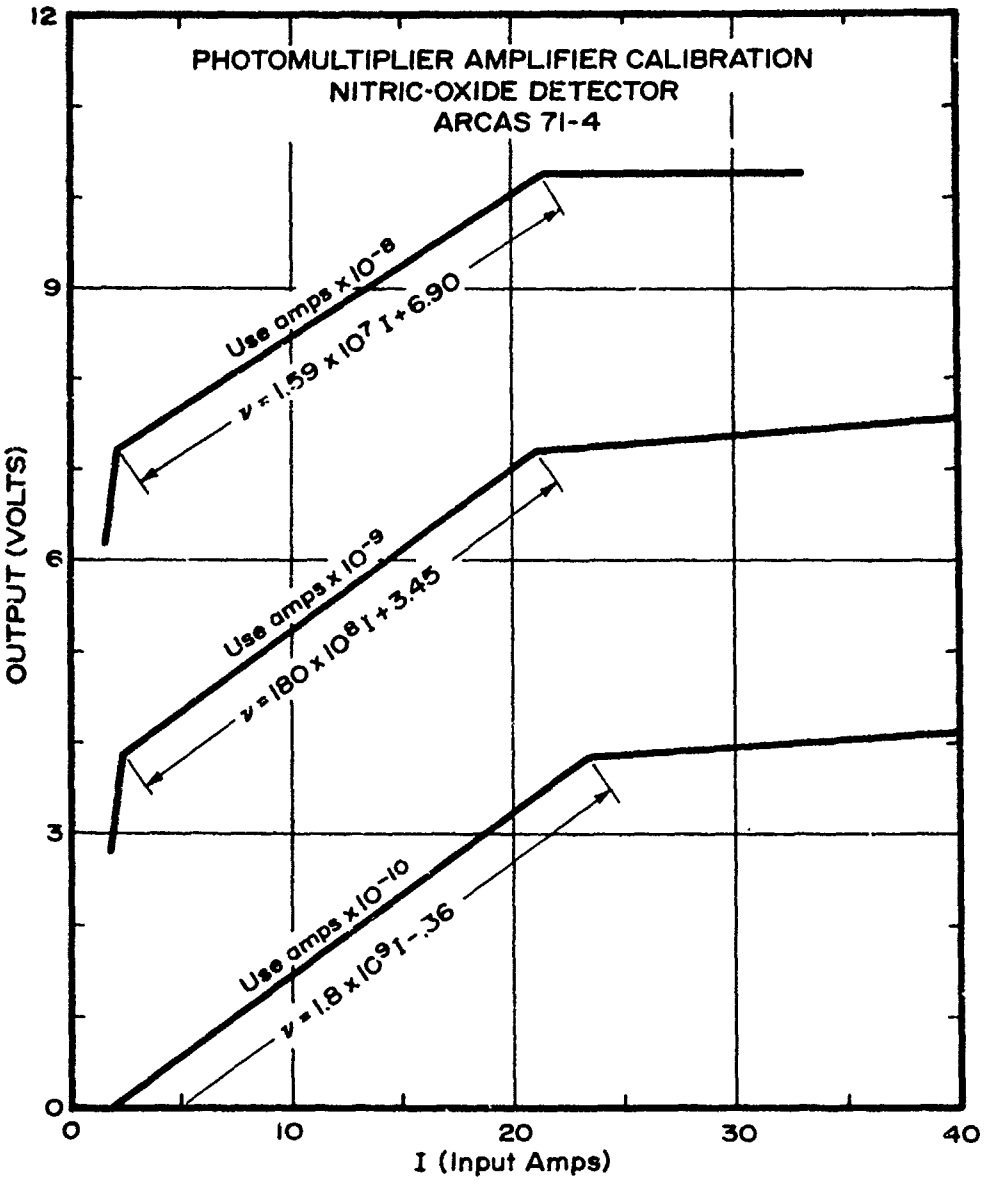

Figure C-5. Nitric oxide detector photomultiplier amplifier calibration, Arcas 71-4.

TABLE C-1

ARCAS 71-4 PHOTOMULTIPLIER AMPLIFIER

GAIN EQUATIONS

Output Range Volts	Function	
0 -- + 3.85	$v = 1.80 \times 10^9 I - .36$	where
+3.85 -- + 7.20	$v = 1.80 \times 10^8 I + 3.45$	I = amplifier input in amperes
+7.20 -- +10.26 (saturation)	$v = 1.59 \times 10^7 I + 6.90$	v = amplifier output in volts

TABLE C-2

ARCAS 71-4 ANALOG TO DIGITAL

CONVERSION FORMAT

Input (volts)	Output Bit Number 8	7	6	5	4	3	2	1
+9.96	1	1	1	1	1	1	1	1
+8.75	1	1	1	0	0	0	0	0
+7.50	1	1	0	0	0	0	0	0
+5.00	1	0	0	0	0	0	0	0
+2.50	0	1	0	0	0	0	0	0
+1.25	0	0	1	0	0	0	0	0
+ .63	0	0	0	1	0	0	0	0
+ .31	0	0	0	0	1	0	0	0
+ .156	0	0	0	0	0	1	0	0
+ .075	0	0	0	0	0	0	1	0
+ .037	0	0	0	0	0	0	0	1

TABLE C-3

MAGNETOMETER S/N 3374 CALIBRATION

ARCAS 71-4

Field (Milligauss)	Output (volts)	
600	4.81	
550	4.61	
500	4.41	
450	4.21	
400	4.01	
350	3.81	
300	3.60	
250	3.40	
200	3.20	
150	3.00	
100	2.79	
50	2.60	
0	2.40	(BIAS LEVEL)
-50	2.20	
-100	2.00	
-150	1.80	
-200	1.60	
-250	1.40	
-300	1.19	
-350	0.99	
-400	0.79	
-450	0.59	
-500	0.39	
-550	0.20	
-600	0.00	

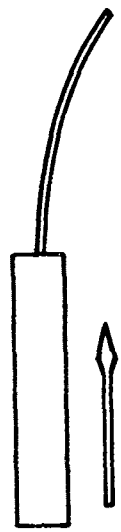

Direction of Magnetic Field for voltage signals above bias level.

TABLE C-4

16 SEGMENT COMMUTATOR ASSIGNMENTS

ARCAS 71-4

Segment	Assignment
1	+5v
2	+5v
3	+5v
4	0v
5	Magnetometer output
6	Magnetometer bias
7	Baroswitch*
8	Cell position monitor**
9	Most significant bit
10	
11	Segments 9-16
12	8 bit binary,
13	number representing
14	photomultiplier amplifier output
15	
16	Least significant bit

Commutator frame rate = 16 frames per second

*Baroswitch closure at 75,000 ft ± 3,000 ft

Altitudes ≤ 75,000 ft = + .8v

Altitudes ≥ 75,000 ft = +3.3v

**Evacuated cell in field of view = + .8v

NO filled cell in field of view = +3.3v

Subcarrier oscillator frequency = 40 KHz

Transmitter Frequency = 1680 MHz